Report No. UT-21.18

INFLUENCE OF WINGWALL GEOMETRY AND SKEW ANGLE ON PASSIVE FORCE BEHAVIOR OF BRIDGE ABUTMENTS FROM LARGE-SCALE TESTING

Prepared For:

Utah Department of Transportation
Research & Innovation Division

Final Report

June 2021

RESEARCH
UDOT Keeping Utah Moving
Utah Department of Transportation - Research Division
4501 South 2700 West - P.O. Box 148410 - SLC,UT 84114-8410

DISCLAIMER

The authors alone are responsible for the preparation and accuracy of the information, data, analysis, discussions, recommendations, and conclusions presented herein. The contents do not necessarily reflect the views, opinions, endorsements, or policies of the Utah Department of Transportation or the U.S. Department of Transportation. The Utah Department of Transportation makes no representation or warranty of any kind, and assumes no liability therefore.

ACKNOWLEDGMENTS

Funding for this study was provided through the Transportation Pooled Fund Program study number TPF-5(264) "Passive Force-Displacement Relationships for Skewed Abutments" supported by the Federal Highway Administration (FHWA, USDOT) and the state departments of transportation of California, Minnesota, Montana, New York, Oregon, Utah, and Wisconsin, along with their structural/geotechnical engineering contacts. The Utah Department of Transportation served as the lead agency for the pooled fund study, with Darin Sjoblom as the geotechnical champion and David Stevens as the research project manager. This support is gratefully acknowledged; however, the conclusions and recommendations in this report do not necessarily represent those of the sponsoring organizations. We also express our appreciation to the Salt Lake City Airport Department for providing access to the test site used for this study.

UNIT CONVERSION FACTORS

In some cases, units used in this report are listed in both the U.S. Customary system and the International System of Units (SI). For the few instances where units used in this report do not conform to the UDOT standard unit of measurement (U.S. Customary system) and are not listed in both systems of units, the units are given below with their U.S. Customary equivalents:

- 1 kilopascal (kPa) = 0.01 ton per square foot (tsf) = 0.02 kip per square foot (ksf)

TECHNICAL REPORT ABSTRACT

1. Report No. UT-21.18	2. Government Accession No. N/A	3. Recipient's Catalog No. N/A
4. Title and Subtitle INFLUENCE OF WINGWALL GEOMETRY AND SKEW ANGLE ON PASSIVE FORCE BEHAVIOR OF BRIDGE ABUTMENTS FROM LARGE-SCALE TESTING		5. Report Date June 2021 6. Performing Organization Code N/A
7. Author(s) Kyle M. Rollins, Aaron Marsh, Kyle Smith, Bryan Franke, Katie McKay, Jaycee Smith, Amy Fredrickson, and Josh Curtis		8. Performing Organization Report No. N/A
9. Performing Organization Name and Address Brigham Young University Dept. of Civil and Environmental Engineering Engineering Building 430 Provo, UT 84602		10. Work Unit No. 42051 15D 11. Contract or Grant No. 13-8123
12. Sponsoring Agency Name and Address Utah Dept. of Transportation (lead agency for TPF-5(264)) 4501 South 2700 West P.O. Box 148410 Salt Lake City, UT 84114-8410		13. Type of Report & Period Covered Final Report Aug. 2012 to Dec. 2020 14. Sponsoring Agency Code PIC No. UT11.406
15. Supplementary Notes Prepared in cooperation with the Utah Department of Transportation, the U.S. Department of Transportation, Federal Highway Administration, and the other state DOTs contributing to the Transportation Pooled Fund Program study number TPF-5(264), with Utah DOT being the lead agency for the pooled fund study.		

16. Abstract

This report summarizes the results of the testing and analyses performed for the large-scale tests of Phase I of the TPF-5(264) pooled fund study. Detailed reports on each of the large-scale tests are available from the Utah Department of Transportation Research & Innovation Division and the TPF-5(264) study webpage. A series of large-scale passive force-deflection tests were performed on a simulated bridge abutment to investigate the effect of wingwall geometry and skew angle on passive force behavior. Tests were conducted at abutment skew angles of 0°, 15°, 30°, and 45° with a backwall that was 11 feet wide and 5.5 feet tall. Backfills included sand and sandy gravel compacted to 95% of the modified Proctor maximum dry unit weight. Wingwalls included concrete walls normal to and parallel to the abutment backwall, as well as Mechanically Stabilized Earth (MSE) wall panels normal to the backwall. For wingwalls transverse to the direction of travel, shear planes extended beyond the abutment walls increasing the effective width of the abutment in a 3D failure geometry. In this case, passive force was best estimated using a triaxial friction angle with the log-spiral method. For MSE wingwalls parallel to the direction of travel, shear planes followed the wingwalls and developed a 2D failure geometry. Passive force was best estimated using a plane strain friction angle with the log-spiral method, in this case. Test results indicate that the passive force decreases significantly as the abutment skew angle increases to 45° relative to non-skewed walls. The results also indicate that the reduced passive force can be accounted for using a simple reduction factor that is a function of skew angle. The skew reduction factor was relatively consistent for all soil types, wingwall styles, and backfill width-to-height ratios investigated. Displacement required to develop the peak passive force was about 3 to 5% of the wall height regardless of skew angle for sand and about 6% for gravel. Normalized passive force vs. normalized displacement curves for all skew angles in sand plotted in a narrow band with the shape of a hyperbola. Some additional conclusions are shared in this summary report.

17. Key Words Abutments, Bridges, Lateral Resistance, Passive Force, Seismic Design, Skewed Abutments, Wingwalls		18. Distribution Statement Not restricted. Available through: UDOT Research & Innovation Div. 4501 South 2700 West P.O. Box 148410 Salt Lake City, UT 84114-8410 www.udot.utah.gov/go/research		23. Registrant's Seal N/A
19. Security Classification Unclassified	20. Security Classification Unclassified	21. No. of Pages 45	22. Price N/A	

TABLE OF CONTENTS

LIST OF TABLES

LIST OF FIGURES

EXECUTIVE SUMMARY

This report summarizes the results of the testing and analyses performed for the large-scale tests of Phase I of the TPF-5(264) pooled fund study. Detailed reports on each of the large-scale tests are available from the Utah Department of Transportation Research & Innovation Division and the TPF-5(264) study webpage.

A series of large-scale passive force-deflection tests were performed on a simulated bridge abutment to investigate the effect of wingwall geometry and skew angle on passive force behavior. Tests were conducted at abutment skew angles of 0°, 15°, 30°, and 45° with a backwall that was 11 feet wide and 5.5 feet tall. Backfills included sand and sandy gravel compacted to 95% of the modified Proctor maximum dry unit weight. Wingwalls included concrete walls parallel and transverse to the direction of travel, as well as Mechanically Stabilized Earth (MSE) wall panels parallel to the direction of travel. For wingwalls transverse to the travel direction, shear planes extended beyond the abutment walls increasing the effective width of the abutment in a 3D failure geometry. In this case, passive force was best estimated using a triaxial friction angle with the log-spiral method. For wingwalls parallel to the travel direction, shear planes followed the wingwalls and developed a 2D failure geometry. Passive force was best estimated using a plane strain friction angle with the log-spiral method, in this case. Test results indicate that the passive force decreases significantly as the abutment skew angle increases to 45° relative to non-skewed walls. The results also indicate that the reduced passive force can be accounted for using a simple reduction factor that is a function of skew angle. The skew reduction factor was relatively consistent for all soil types, wingwall styles, and backfill width-to-height ratios investigated. Displacement required to develop the peak passive force was about 3 to 5% of the wall height regardless of skew angle for sand and 6% for gravel. Normalized passive force vs. normalized displacement curves for all skew angles in sand plotted in a narrow band with the shape of a hyperbola. Some additional conclusions are shared in this summary report.

1.0 INTRODUCTION

Passive force-deflection behavior must be considered in bridge design to ensure adequate resistance to both seismically and thermally induced forces. Transverse shear force-deflection relationships for the backwall of an abutment are also important. These relationships are typically used to define normal and transverse abutment springs for numerical models. Several researchers have conducted large-scale field studies to investigate passive force-deflection behavior with densely compacted granular backfills for non-skewed abutments (Cole and Rollins, 2006; Duncan and Mokwa, 2001; Lemnitzer et al., 2009; Rollins and Sparks, 2002). The results from these field studies show that the ultimate passive force may be reasonably predicted using the log-spiral method and that it develops at displacements of approximately 3% to 5% of the wall height (Cole and Rollins, 2006; Lemnitzer et al., 2009).

Wingwalls for bridge abutments may consist of reinforced concrete (RC) walls either parallel or perpendicular to the direction of travel or Mechanically Stabilized Earth (MSE) walls parallel to the direction of travel as shown in Fig. 1. Variations in passive resistance based on wingwall geometry are seldom considered, although research indicates that MSE wingwalls produce higher passive force per width because of the plane strain geometry (Heiner et al. 2008, Franke et al. 2013).

Owing to geometrical constraints, bridge abutments are increasingly constructed at a skew to underlying roadways. The national FHWA bridge database indicates that about 40% of the 600,000 bridges in the US are skewed. Skewed bridges experienced twice the damage rate of non-skewed bridges during the 2010 Chilean earthquake (Toro et al., 2013). Nevertheless, most current codes and practices do not distinguish between skewed and non-skewed bridge abutment geometries in computing passive force. Numerical models (Shamsabadi et al. 2006, 2019) and large-scale tests (Rollins and Jessee 2013, Marsh et al. 2013, Franke et al. 2013) suggest a significant reduction in passive force for skewed bridge abutments. Therefore, the increased damage rate of skewed abutments may result from a combination of structural weaknesses and reduced passive resistance.

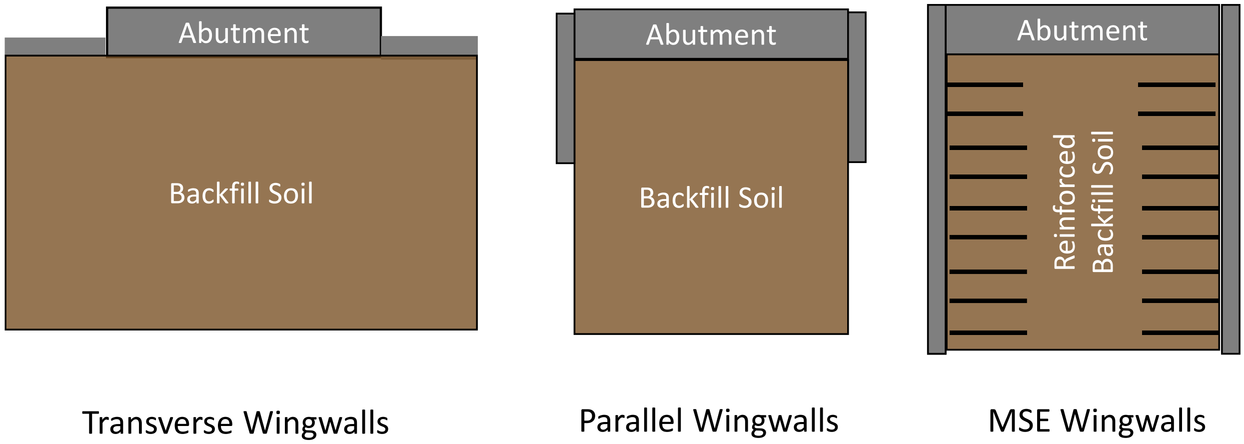

Fig. 1. Schematic illustration of abutment wingwall geometries used in the testing program (plan view).

Based on large-scale lab tests, Rollins and Jessee (2013) proposed the reduction factor, R_{skew}, given in Eq. 1, to account for reduced passive force as a function of skew angle, θ (degrees). This relationship reduces the non-skewed passive force, P_p, for skewed bridge abutments relative to a non-skewed abutment of equivalent width transverse to the direction of travel. Using Eq. 2, this reduction factor can be used to obtain the reduced passive force, $P_{p\text{-}skew}$, for skewed bridge abutments.

$$R_{skew} = 8.0 * 10^{-5}\theta^2 - 0.018\theta + 1.0 \quad (1)$$

$$P_{p-skew} = P_p R_{skew} \quad (2)$$

Because Eq. 1 was based only on lab-scale (4 ft wide and 2 ft high) walls and computer models, the need for additional large-scale testing was apparent. To understand the behavior of skewed abutments and wingwall geometries better, a series of large-scale tests have been performed with skew angles of 0°, 15°, 30°, and 45° using an existing pile cap (11 ft wide by 5.5 ft tall by 15 ft long) to simulate a bridge abutment displacement into adjacent backfill material. Backfill typically consisted of a 6-ft thick layer of densely compacted sand extending about 1 ft below the base of the abutment; however, some tests were also performed using dense compacted sandy gravel, and Geosynthetic Reinforced Soil (GRS) consisting of geotextile sheets with gravel backfill.

Tests were also performed with a variety of wingwall geometries including wingwalls in the following configurations: transverse to the direction of travel, parallel to the direction of travel consisting of MSE walls, and parallel to the direction of travel consisting of tapered reinforced concrete walls.

Because the abutment width-to-height ratio in both the field and lab tests was two, whereas this ratio would be substantially higher for many abutments in practice, another series of tests was performed with the same pile cap width (11 ft) but with a 3-ft thick sand backfill above the base of the abutment which extended 0.5 ft below the abutment. For these tests, the width-to-height ratio was 3.7, nearly doubling the ratio for the original tests. This makes it possible to evaluate the effect of the width-to-height ratio on the skew reduction factor.

The main objective of this report is to summarize the results obtained from these large-scale passive force tests and provide recommendations regarding the effects of wingwall geometry and skew angle on passive force at abutments. In addition, normalized passive force vs. normalized deflection curves are provided. Finally, this report identifies simple procedures to successfully account for the effects of various wingwall configurations on passive force.

This report summarizes the results of the testing and analyses performed for the large-scale tests of Phase I of the TPF-5(264) pooled fund study. Detailed reports on each of the large-scale tests are available from the Utah Department of Transportation Research & Innovation Division and the TPF-5(264) study webpage.

2.0 FORCE EQUILIBRIUM AT ABUTMENT BACKWALL

As a bridge deflects longitudinally into the soil at an abutment, different interaction forces develop between the backwall of the abutment and the adjacent soil for a skewed geometry as shown in the plan view drawing in Fig. 2.

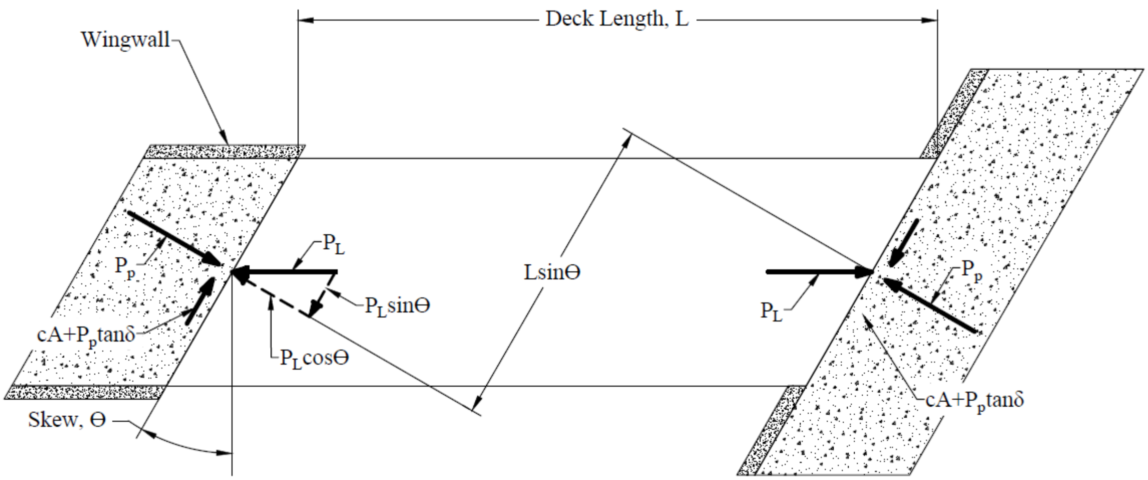

Fig. 2. Plan view of force interaction between bridge structure and skewed abutment.

At the soil-abutment interface, the longitudinal force, P_L, acts parallel to the bridge structure. This longitudinal force may be broken into two components: a component acting normal, $P_L\cos\theta$, and a component acting parallel, $P_L\sin\theta$, to the abutment backwall where θ is the skew angle. The normal force component is resisted by the passive soil resistance, P_p, (see Eq. 3). The parallel component, P_T, (see Eq. 4) is resisted by the soil shear resistance, P_R, provided at the interface between the soil backfill and bridge abutment as defined by Eq. 5, where c is soil cohesion, A is backwall area, and δ is the abutment backwall-soil interface friction angle. As shown in Eq. 5, the shear resistance is directly related to the passive resistance so that a decrease in passive resistance leads to a proportional decrease in shear resistance. Force and moment equilibrium must be maintained as noted by Eqs. 6 and 7 suggested by Burke (1994). In these equations, F_s is the factor of safety and L is the length of the bridge.

For longitudinal forces only:

$$P_p = P_L \cos\theta \tag{3}$$

$$P_T = P_L \sin\theta \tag{4}$$

$$P_R = cA + P_p \tan\delta \tag{5}$$

$$\frac{cA + P_p \tan\delta}{F_s} \geq P_L \sin\theta \tag{6}$$

$$\frac{(cA + P_p \tan\delta) L \cos\theta}{F_s} \geq P_p L \sin\theta \tag{7}$$

3.0 PASSIVE FORCE TESTS AND TEST LAYOUT

Plan and profile drawings of the test layout and wingwall geometries used in the test are provided in Figs. 3 through 5. Fig. 3 provides plots for the test layout with transverse wingwalls relative to the direction of loading. Sand backfill for this test layout was placed to 3 ft and 5.5 ft above the base of the abutment, and wedges were fixed to the pile cap to produce skew angles of 0°, 15°, 30° and 45°. Gravel backfill for this wingwall geometry was placed to a height of 3.5 ft above the abutment base and involved skew angles of 0° and 30°. Fig. 4 shows the test layout with parallel MSE wingwalls, and Fig. 5 shows the test layout for the parallel reinforced concrete (RC) tapered wingwall. Sand backfill heights for the MSE wall were all 5.5 feet above the base of the abutment, and tests were performed with skew angles of 0°, 15°, 30° and 45°. For the parallel tapered wingwalls, the sand backfill was compacted to 5.5 ft above the abutment base, but the backfill was sloped downward at 2H:1V beyond the sides of the wingwalls and against the outside of the wingwalls. Test were only performed for 0° and 45° skew angles in this case. A summary of the wingwall geometry, skew angles, and backfill properties for all the passive force tests performed during this study is provided in Table 1.

As shown in Fig. 3, an existing 11-ft wide by 5.5-ft tall by 15-ft long pile cap was used as a large-scale model of an abutment backwall for the passive force tests. The cap was supported vertically by two rows of three 12.75-in outside diameter closed-ended steel piles extending about 43 ft (13.1 m) below the ground surface. As shown in Fig. 3, load was applied in the longitudinal direction by two 600-kip MTS hydraulic actuators, that pushed the pile cap into the compacted backfill. The reaction for the actuators was provided by two 4-ft diameter shafts and a sheet pile wall tied together with tie-rods between two 5-foot deep beams. The backfill zone behind the pile cap was approximately 22 ft wide and extended 24 ft longitudinally from the backwall (pile-cap) face for the 0° skew test. However, because additional concrete wedges were attached to the existing pile cap to produce a skewed abutment backwall, the backfill eventually extended approximately 24 ft longitudinally from the acute corner of the skewed abutment. Furthermore, the base of the test pit was excavated approximately 1.0 ft below the bottom of the pile-cap and extended 10 ft longitudinally from the backwall face. This prevented any interference from the native soil in the development of a potential log-spiral failure surface.

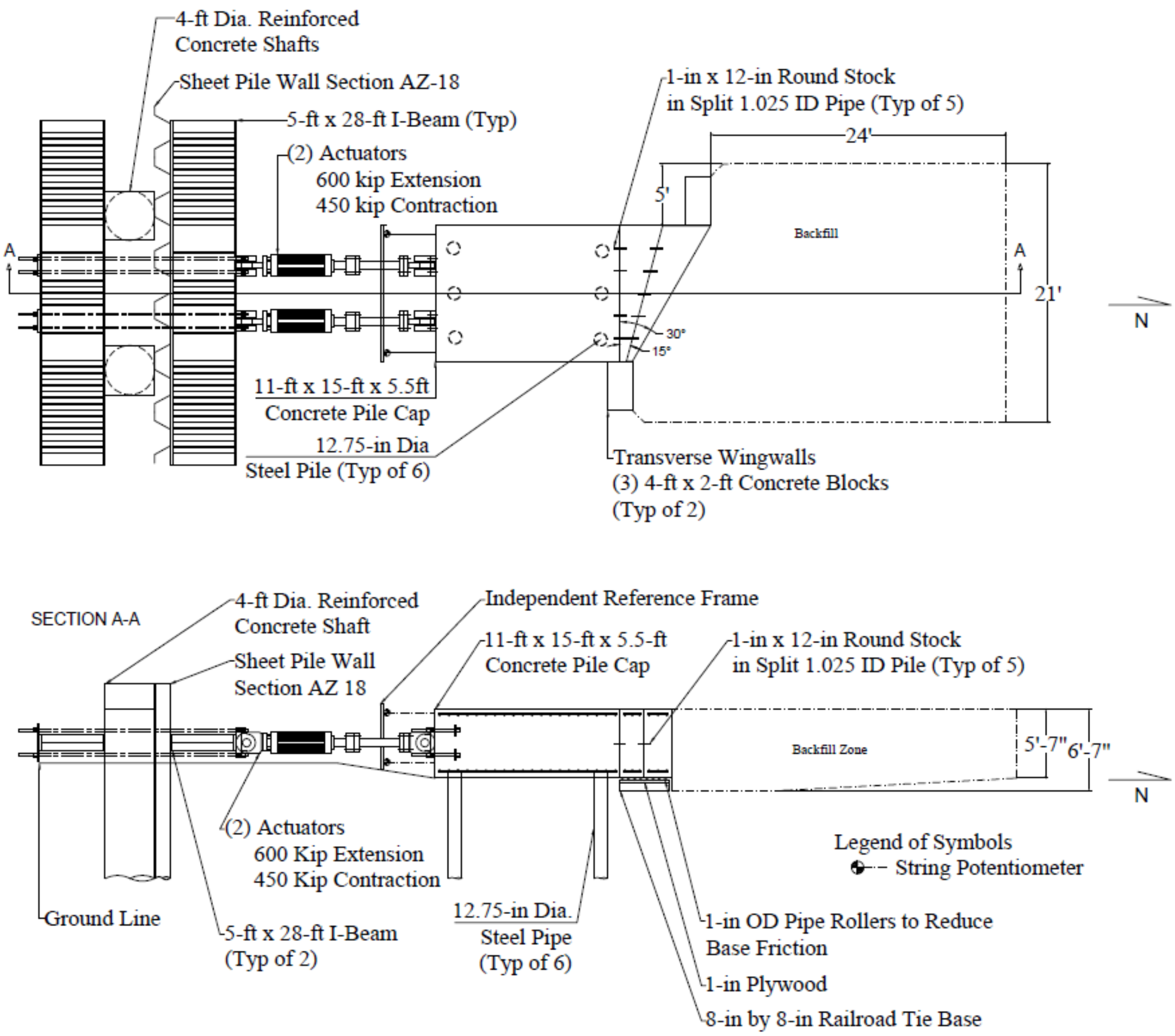

Fig. 3. Plan and profile views of the test abutment, backfill, and loading system for wingwalls transverse to the direction of travel.

In addition to attaching concrete wedges to the pile-cap face for the 15°, 30°, and 45° skew tests, the concrete wedges were placed atop a set of steel rollers resting on a small wooden platform beneath the concrete wedge. This minimized friction between the concrete wedge and the underlying soil. In addition, it ensured that lateral resistance was due only to the passive soil resistance provided by the backfill material and the piles beneath the existing pile cap. Testing with no backfill showed a small increase in lateral resistance as a result of each additional concrete wedge.

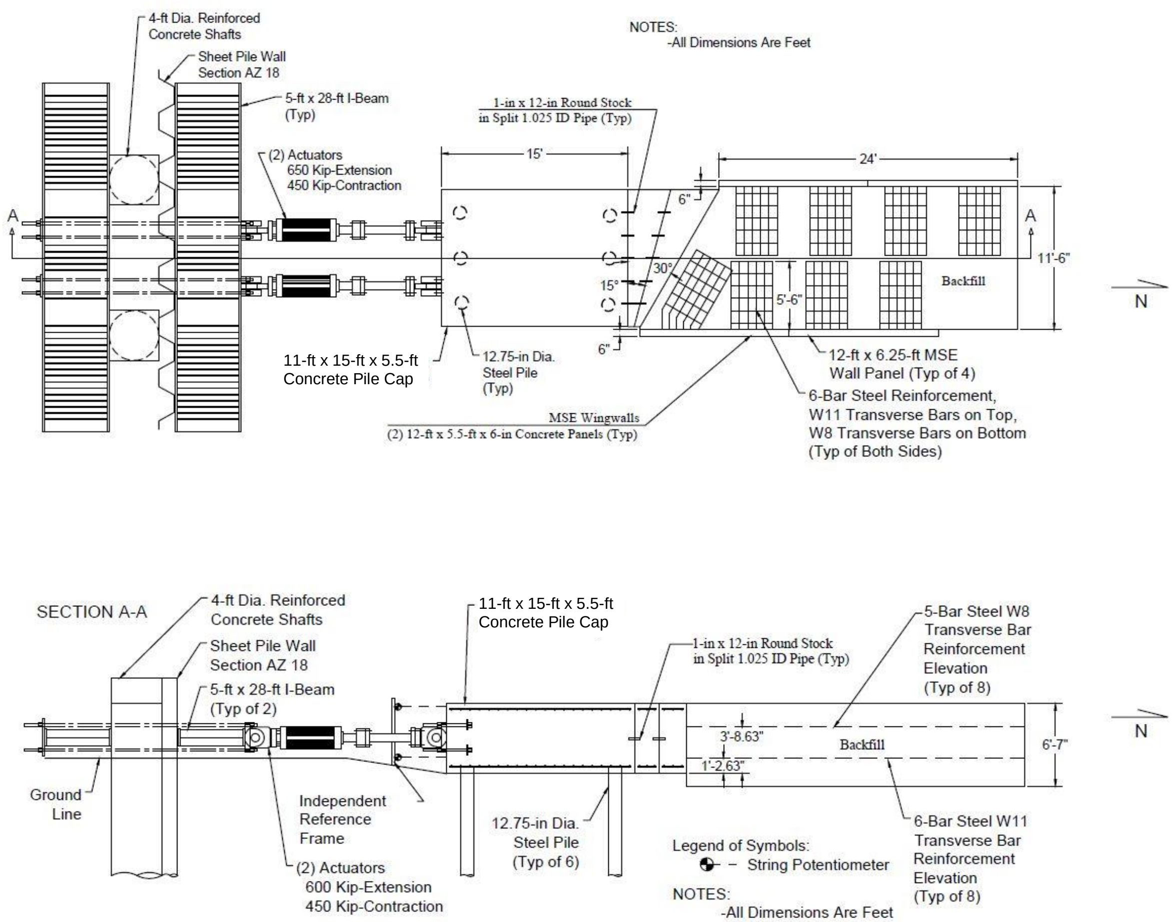

Fig. 4. Plan and profile views of the test abutment, backfill, and loading system with MSE wingwalls parallel to the direction of travel.

The lateral load tests were performed using a displacement-controlled approach. Loads were applied to the two actuators sufficient to produce uniform longitudinal displacement increments of about 0.25 inch up to a maximum displacement of about 3 to 4 inches. Although this procedure kept pile cap rotation at very small levels, some transverse displacement of the cap did take place which was usually less than 0.3 inch. Prior to conducting tests with backfill in place, lateral load tests were performed on the pile cap without backfill in place to determine the "baseline" force-deflection relationship produced by the piles and cap block alone. After placement of the backfill, the longitudinal force measured by the actuators was reduced by the lateral resistance provided by the piles and cap using the baseline curves for each test. For the 15°, 30°, and 45° skew tests, the passive force was then computed from the net longitudinal force using Eq. 3.

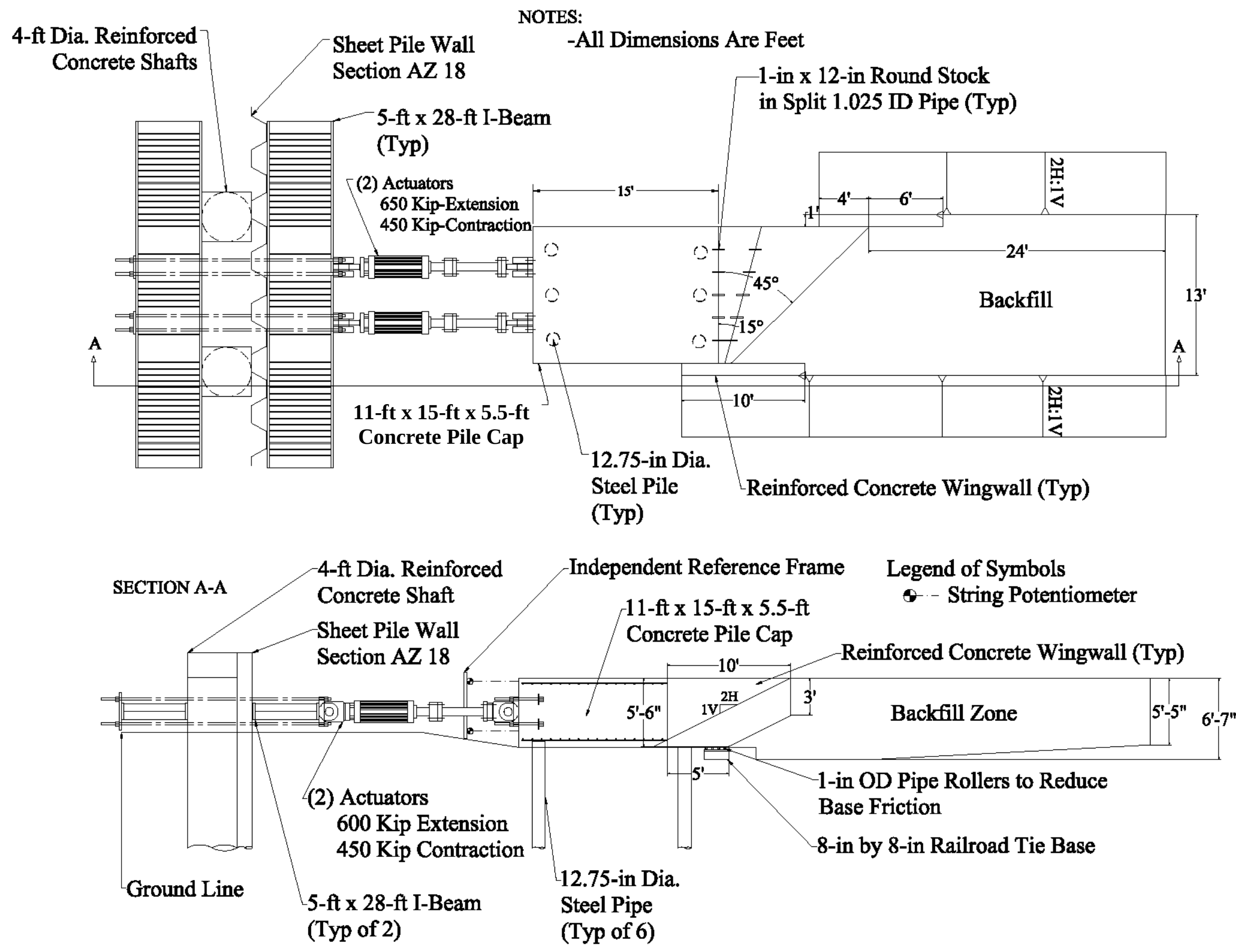

Fig. 5. Plan and profile views of the test abutment, backfill, and loading system with tapered reinforced concrete (RC) wingwalls parallel to the direction of travel.

Table 1. A summary of the wingwall geometry, the skew angles, and backfill properties for the passive force tests performed during this study.

Test No	Wingwall Type	Skew Angle θ (Degrees)	Backfill Height H (ft)	Width/ Height (W/H)	Soil Type	Avg. Dry Unit Wt. γ_d (lbs/ft^3)	Avg. Water Content w (%)	Avg. Relative Compaction R_c (%)	Avg. Relative Density Dr (%)	Skew Reduction Factor R_{skew} (Fraction)	Failure Deflection (% of H)
1	Transverse	0	5.5	2	Sand	107.0	8.9	96.0	80	1.00	4.1
2	Transverse	15	5.5	2	Sand	108.3	9.5	97.1	86	0.73	3.0
3	Transverse	30	5.5	2	Sand	108.3	8.3	97.1	86	0.58	3.0
3	Transverse	45	5.5	2	Sand	109.1	9.0	98.3	92	0.36	4.5
4	Transverse	0	3.0	3.67	Sand	107.0	9.2	96.0	81	1.00	3.8
5	Transverse	15	3.0	3.67	Sand	108.0	9.2	96.9	85	0.71	3.4
6	Transverse	30	3.0	3.67	Sand	107.5	9.6	96.4	82	0.45	2.8
7	Transverse	45	3.0	3.67	Sand	109.2	7.1	97.9	90	0.35	2.6
8	MSE Parallel	0	5.5	2	Sand	107.5	9.1	96.4	82	1.00	5.0
9	MSE Parallel	15	5.5	2	Sand	108.5	8.9	97.3	87	0.62	4.8
10	MSE Parallel	30	5.5	2	Sand	108.0	9.2	96.9	84	0.49	4.8
11	MSE Parallel	45	5.5	2	Sand	109.7	9.2	98.4	92	0.29	5.0
12	RC Parallel	0	5.5	2	sand	108.2	7.2	97.0	85	1.00	4.6
13	RC Parallel	45	5.5	2	Sand	109.6	7.8	98.2	92	0.45*	4.5
14	Transverse	0	3.5	3.1	Gravel	136.2	6.4	95.9	80	1.00	5.8
15	Transverse	30	5.5	2.0	Gravel	137.3	7.8	96.7	84	0.58	7.2
16	Transverse	0	3.5	3.1	Gravel/GRS	135.1	5.8	96.2	81	1.00	7.2
17	Transverse	30	3.5	3.1	Gravel/GRS	136.2	6.6	96.9	85	0.63	7.2

*0.45 for 11 ft wide abutment wall that reduces effective skew angle. Numerical analyses indicate value of 0.35 for wider abutment walls.

3.1 Backfill Characterization

Backfill soil used in most of the tests consisted of poorly graded sand, classifying as SP based on the Unified Soil Classification System (USCS) or A-1-b type soil by the AASHTO Soil Classification System. Four tests were also performed using a backfill consisting of well-graded gravel with silt and sand, classifying as GW-GM according to the USCS or A-1-a according to the AASHTO classification system. Gradation curves for the sand and gravel are provided in Fig. 6.

The maximum dry unit weight and optimum moisture content for the sand were determined to be 111.5 lb/ft^3 and 7.1%, respectively, from the modified Proctor compaction test (ASTM D1557). For the gravel, the maximum dry unit weight according to the modified Proctor compaction test (ASTM D1557) was 142.0 lb/ft^3 and the optimum moisture content was 6.3%. Compaction was performed using a vibratory, smooth-drum roller compactor to compact 6-in lifts of backfill material along with a plate compactor and jumping jack compactors near the wall face. The objective was to achieve an average relative compaction greater than about 96%. Throughout testing, a calibrated nuclear density gauge was used to ensure proper compaction and moisture content. A summary of the average dry unit weights, water contents, and relative compaction for each backfill test is provided in Table 1 along with an estimation of relative density using a correlation developed by Lee and Singh (1971).

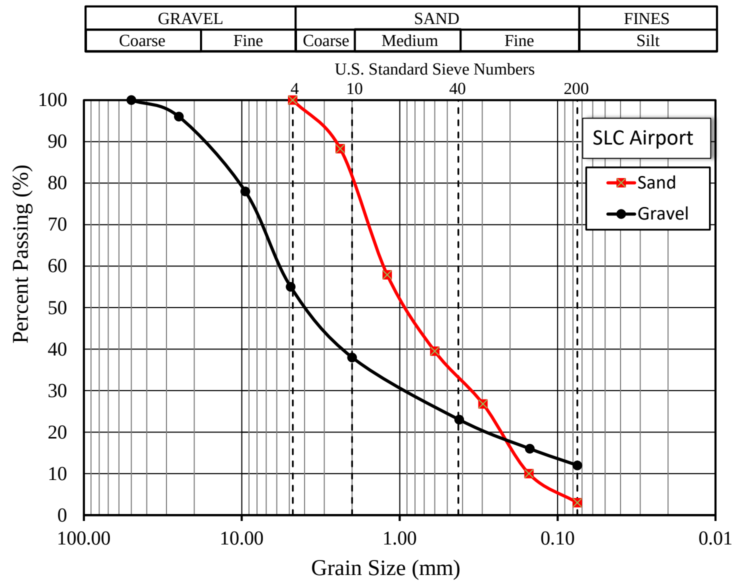

Fig. 6. Grain size distribution curves for sand and gravel backfill used in field tests.

For two of the gravel tests, geotextile fabric layers were placed betweeen every 1-ft compacted gravel layer starting at 6 inches below the base of the cap. The fabric was initially laid flat so that the extra fabric on the sides and against the backwall came up vertically. The fill was then placed on top of the geofabric sheets. At each 1-ft interval, the fabric against the interface from the previous layer was folded over the fill before placing the new layer of fabric. The fabric was placed such that there was at least 3 ft of fabric lying on top of the gravel before the next layer was placed. Therefore, the resulting interface between the backfill and the pile cap wall was completely geotextile fabric.

The geotextile sheets for the GRS tests were Mirafi® RS380i which was donated by Tencate Geosynthetics Americas for this research project. This geotextile is woven from polypropylene (PP) filaments to provide desired strength and soil retention characteristics along with high water flow capacity. Based on test results from the manufacturer, the geotextile has a minimum tensile modulus of 51,000 lb/ft (744 kN/m), which equates to a tensile strength of 2,550 lb/ft (37 kN/m) at a strain of 5%. The geotextile has an apparent opening size (AOS) equivalent to a #40 U.S. sieve size (0.43 mm).

Triaxial shear and direct shear tests indicate that the drained friction angle (ϕ') for the compacted sand is between 40° and 42°, and the wall friction angle (δ) between the concrete wall and the sand is 0.65 to 0.75 times ϕ'. In situ direct shear tests were performed on the compacted sand and gravel backfills in the field. The drained friction angle was found to be 45.8° with a cohesion of 40 lb/ft^2 (psf) for the gravel and 41.9° with a cohesion of 100 lb/ft^2 (psf) for the sand. Laboratory direct shear interface friction tests between the geosynthetic sheet and the concrete backwall found an interface friction angle (δ) to be 26.1° or 0.57 of ϕ'.

3.2 Instrumentation

Two MTS hydraulic actuators were used to apply and measure longitudinal forces during testing. Four string potentiometers attached to the back side of the pile cap measured longitudinal pile-cap displacement relative to an independent reference beam. Longitudinal displacement of the pile cap was confirmed using independent measurements from inclinometer and shape array readings taken at both the north and south ends of the pile cap. Inclinometers and shape arrays were installed to a depth of 40 feet in the middle pile in the front and back rows of piles in the cap to monitor the longitudinal and transverse movement of the cap and piles during lateral loading.

Before testing, a grid of 2.0-ft squares, refined to a grid of 1.0-ft squares near the backwall, was painted on the surface of the backfill to determine vertical heave and horizontal displacement. Measurements at each grid-intersection point were made using an auto level and total station survey before and after each test. A series of string potentiometers were also used to monitor the compression of the backfill relative to the face pile cap at 2 ft intervals in front of the cap.

On the 30° and 45° skew wedges, six “fat back” pressure cells, manufactured by Geokon, were cast flush with the face of the wedge at a depth of 3.67 ft below the top of the wall. These cells measured earth pressure exerted on the front face of the wedge by the adjacent backfill as the pile cap was pushed longitudinally into the backfill soil.

Finally, vertical columns of red sand were installed in the sand backfill at various depths behind the pile cap to identify the location of the passive shear planes with distance from the pile cap. After fill placement, 2-inch diameter holes were hand-augered through the backfill and replaced by compacted red sand. After testing, trenchs were excavated adjacent to the columns to observe the location where the columns were offset by the shear planes.

4.0 EFFECT OF WINGWALL GEOMETRY ON PASSIVE FORCE-DEFLECTION CURVES

Passive force-deflection curves for the abutments with transverse wingwalls, parallel MSE wingwalls, and parallel tapered RC wingwalls are plotted in Fig. 7 for the no-skew case. The transverse wingwall geometry produced the highest passive force for a given deflection, while the tapered RC wingwall produced the lowest passive force. The higher passive force for the abutment with transverse wingwalls is largely a result of the larger effective width of the passive failure wedge relative to the parallel wingwalls.

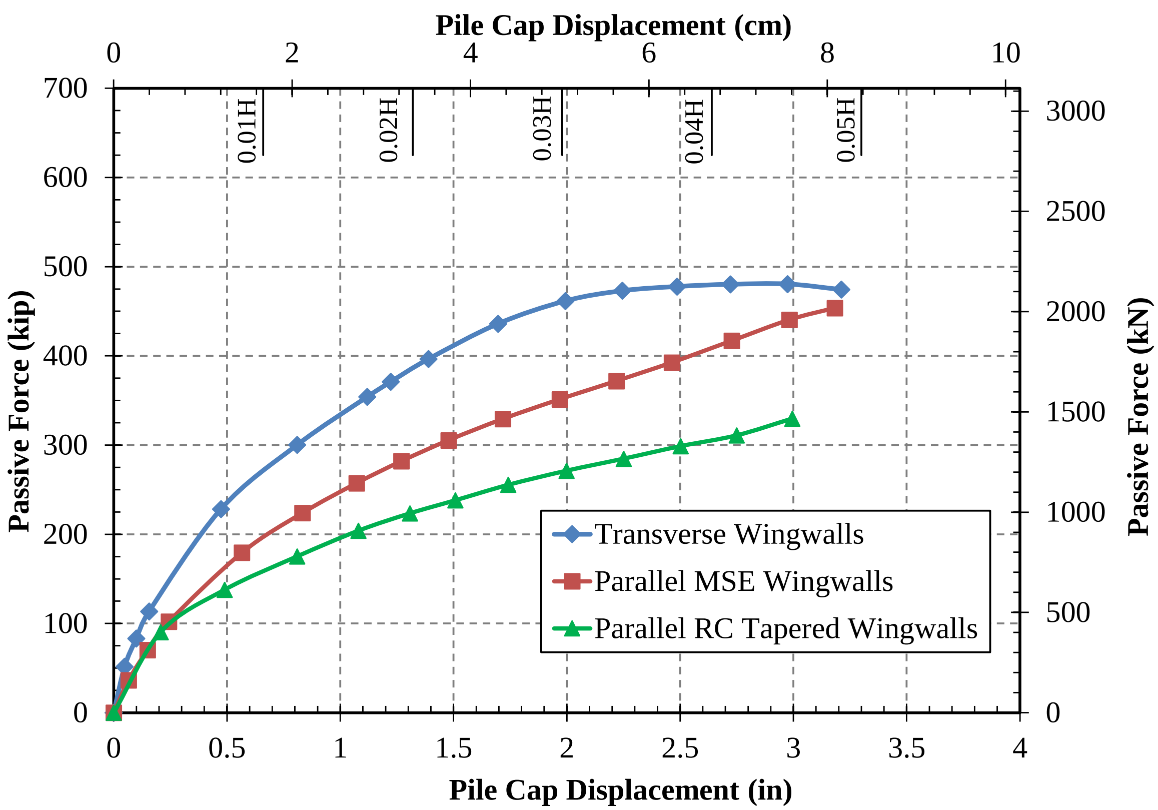

Fig. 7. Passive force-deflection curves for pile cap with transverse wingwalls, parallel MSE wingwalls, and parallel tapered reinforced concrete wingwalls with no skew.

Fig. 8 provides plots of the effective width of the passive failure surface along with color contours of ground heave for abutments with transverse wingwalls, parallel MSE wingwalls, and parallel tapered RC wingwalls with no skew. The failure surfaces for the two abutments with parallel wingwalls are similar to the width of the wingwalls with widths of 11.5 ft and 13.5 ft.

However, the failure surface for the pile cap with transverse wingwalls extends far beyond the 11-ft width of the pile cap and develops an effective width of 21 ft as shown in Fig. 8. The passive failure wedge for the transverse wingwall develops a 3D failure surface while the parallel MSE wingwall produces a 2D failure surface.

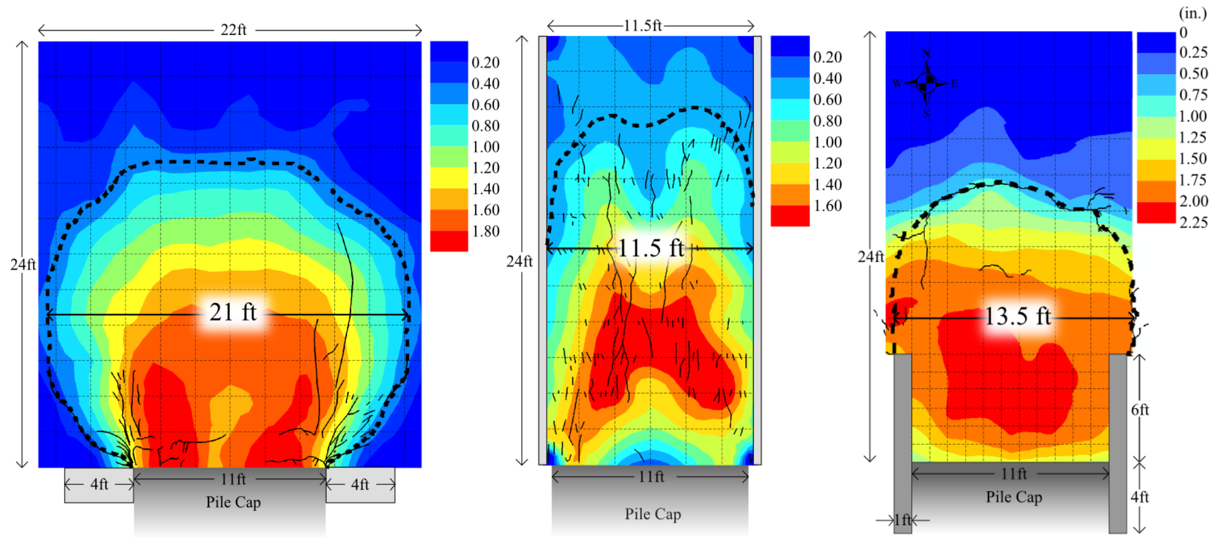

(a) (b) (c)

Fig. 8. Effective width of failure surface along with color contours of ground heave for abutments with (a) transverse wingwalls, (b) parallel MSE wingwalls, and (c) parallel tapered reinforced concrete wingwalls with no skew pushed into the sand backfill.

To provide a better comparison of passive resistance, the passive force per width was calculated by dividing by the effective widths identified in Fig. 8 in each case. Plots of the passive force per width vs. longitudinal deflection are shown for the three wingwall types in Fig. 9. The MSE wingwall geometry provides an additional 60% of passive resistance per width compared to the tapered RC wingwall and transverse wingwall geometries. The increased passive resistance for the parallel MSE wingwalls is likely attributable to the 2D failure geometry for which a plane strain friction angle (ϕ_{PS}) would be applicable, while a triaxial friction angle (ϕ_T) would be more applicable for the 3D failure geometry observed for the transverse wingwall. Kulhawy and Mayne (1990) observed that ϕ_{PS} is on average 12% higher than the triaxial friction angle (ϕ_T) for densely compacted material. Based on a triaxial friction angle of 40°, the plane strain friction angle would then be approximately 44.8°, which would lead to a substantial increase in the passive resistance.

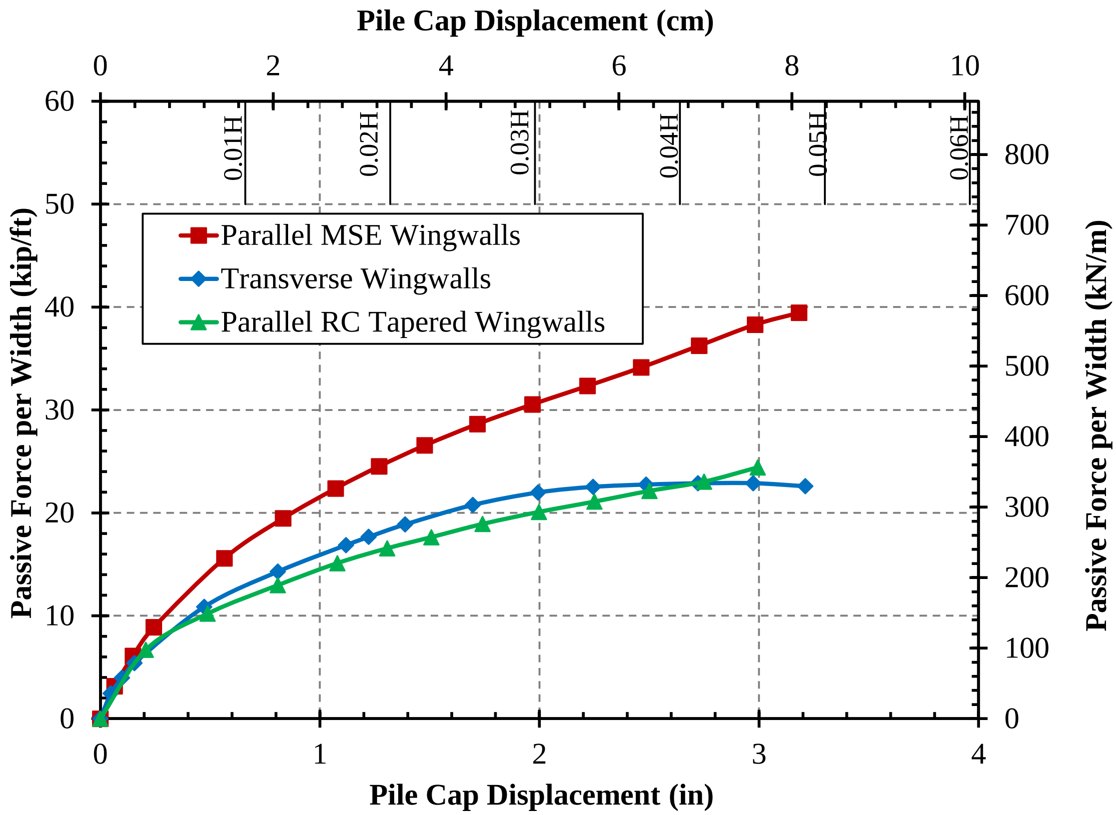

Fig. 9. Passive force per width vs. deflection curves for various wingwall geometries for non-skewed abutments.

The ultimate horizontal passive force (P_{ph}) for each wingwall case has been computed using the equation

$$P_{ph} = (0.5\gamma H^2 K_p B R_{3D} + 2cK_p^{0.5} B R_{3D}) \cos\delta \tag{8}$$

where:

B = Abutment width
H = Abutment height
γ = Backfill moist unit weight
ϕ = Backfill drained friction angle
c = drained cohesion
δ = Wall friction angle
K_p = Passive earth pressure coefficient from log-spiral method
R_{3D} = 3D width correction factor
$B_e = BR_{3D}$ = the effective width of the passive shear wedge

The 3D correction factor, R_{3D} can be computed using the equation proposed by Brinch Hansen:

$$R_{3D} = \left[1 + \left(K_p - K_a\right)^{0.67}\left(1.1A^4 + \frac{1.6}{1 + 5\left(\frac{B}{H}\right)} + \frac{0.4\,(K_p - K_a)\,A^3}{1 + 0.05\left(\frac{B}{H}\right)}\right)\right] \tag{9}$$

where:

A = 1 – (H/z)
z = depth to the base of the abutment wall from the ground surface
K_a = Rankine active earth pressure coefficient, and
K_p = Rankine passive earth pressure coefficient.

The values used in calculating the passive force for each wingwall geometry are summarized in Table 2 along with the computed horizontal passive force and the prediction error relative to the measured passive force.

Table 2 Summary of wall and soil properties used for computing horizontal passive force.

Wingwall Type	Wall Width, B (ft)	Wall Height H (ft)	Cohesion, c (psf)	Friction angle, Φ (degrees)	Wall Friction, δ (degrees)	Moist unit weight, γ (pcf)	3D factor, R_{3D}	Passive earth pressure coefficient, K_p	Horizontal Passive Force, P_{ph} (kips)	% Error
Transverse	11	5.5	100	40	28	117	1.79	12.86	485	2
Parallel MSE	11.5	5.5	100	44.8	31.4	117	1.0	21.76	448	1
Parallel Tapered	13	5.5	100	40	28	117	1.0	12.86	310	3

The drained cohesion of 100 psf for the backfill is attributable to matric suction effects. As noted previously, the plane strain friction angle was used for the parallel MSE wall case, and the triaxial friction angle was used for the other wall types. Wall friction was taken as 0.7 times the friction angle of the backfill based on interface shear tests. As noted in Table 2, the agreement between measured and computed resistance is remarkably good in all cases with errors less than a few percentage points.

5.0 EFFECT OF SKEW ANGLE ON PASSIVE FORCE-DEFLECTION CURVES

5.1 Tests with Wingwalls Transverse to Direction of Travel

Passive force-deflection curves for 0°, 15°, 30°, and 45° skew tests with the transverse wingwall geometery (see Fig. 3) are shown in Figs. 10 and 11 for backfill depths of 5.5 and 3.0 ft above the base of the abutment wall, respectively. A comparison of the maximum passive force for the tests on the skewed abutments shows a significant and progressively greater reduction in the peak passive force as the skew angle increases. For example, the reduction in passive resistance is approximately 50% for the abutments at the 30° skew angle relative to the non-skewed abutment. Despite this fact, the initial soil stiffness appears to be less affected by the skew angle of the abutment at small displacements less than about 0.2 inch. However, the load-deflection curves begin to diverge and show a reduction in stiffness as the ultimate passive resistance is approached, in comparison to the 0° skew test. The two backfill heights showed similar reductions in passive force with respect to skew angle.

Generally, the maximum passive force was obtained with a longitudinal deflection of approximately 3 to 4% of the wall height, and no trend was evident with respect to skew angle. These displacements at failure are consistent with other large-scale passive force-deflections tests (Rollins et al. 2006).

The post-peak passive force decreases to varying degrees for the eight tests over the displacement range which extends to a normalized displacement of 0.09H for the 3-ft high backfill. Greater post-peak reductions are observed for the higher normalized displacements.

Post-peak strength reduction typically occurs when relative compaction reaches 97% of the modified Proctor value (see Table 1). This variation from 95% relative compaction is small and within the range expected for field compaction. Some post-peak strength decrease would be expected for a compacted granular fill as unit weight increased at low confining pressure owing to dilation. Soil dilation during shearing produces a peak resistance followed by decreased soil resistance as the unit weight decreases with continued displacement.

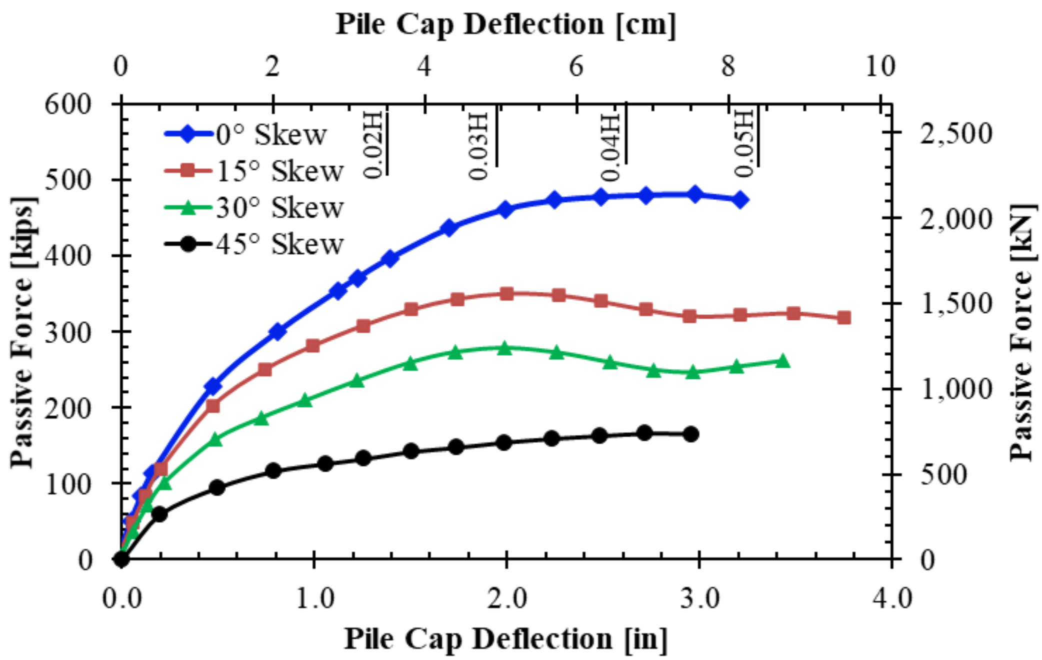

Fig. 10. Passive force-deflection curves for 0°, 15°, 30°, and 45° skew tests with 5.5-ft thick compacted sand backfill and wingwalls transverse to direction of travel.

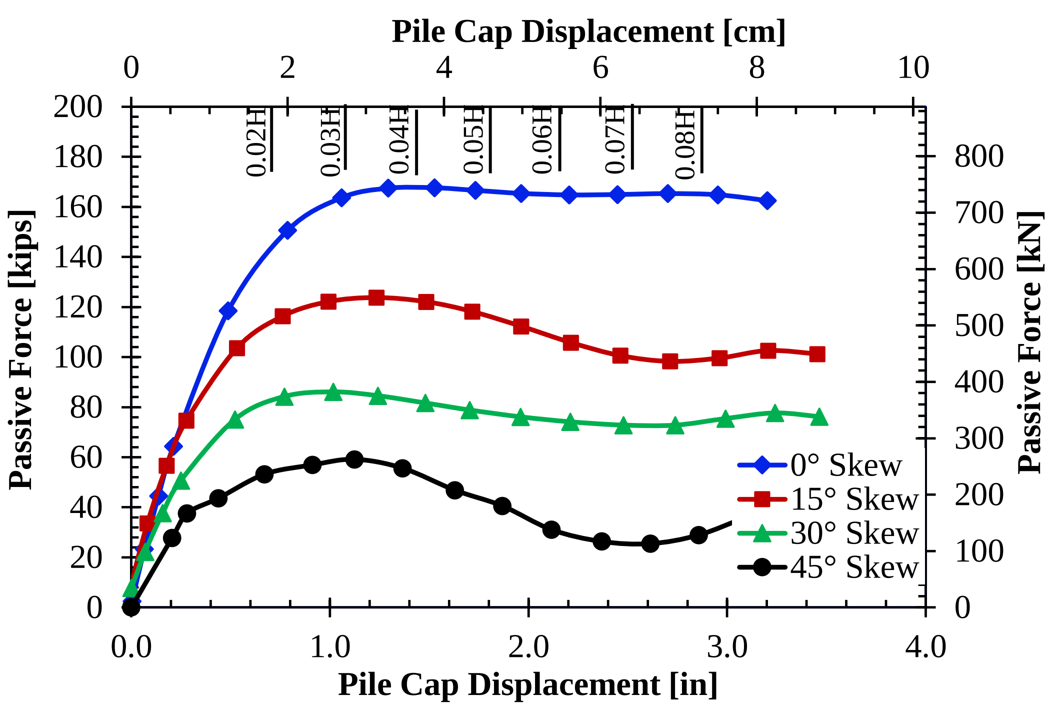

Fig. 11 Passive force-deflection curves for 0°, 15°, 30°, and 45° skew tests with 3.0-ft thick compacted sand backfill and wingwalls transverse to direction of travel.

5.2 Tests with MSE Wingwalls Parallel to Direction of Travel

Passive force-deflection curves for 0°, 15°, 30°, and 45° skew tests with the MSE wingwall geometry (see Fig. 4) are shown in Fig. 12. For the 0° skew test, the longitudinal force reached the capacity of the actuators. Consequently, the passive force did not peak and decline, and the maximum passive force was assigned to the last displacement increment. Because this displacement was approximately 5% of wall height, it is likely very close to the peak value, because all full-scale tests in sand have failed at displacement less than this. As in the case for the transverse wingwalls, the passive force progressively decreased as skew angle increased, and the passive force for the 30° skew was about 50% of that for the 0° skew test. For the tests at 15°, 30°, and 45° skew, the peak passive force also developed at a deflection equal to about 0.05H; however, the curves were relatively flat after a displacement of 0.03H.

For the zero skew test, the MSE walls only deflected outward (transversely) about 0.25 inch until abutment displacement exceeded 0.03H, and the displacement was symmetrical on both sides. At peak passive force with abutment displacements of 0.05H, the outward MSE wall displacement had reached about 1 inch. Horizontal pressure on MSE walls increased with increased passive force and deflection of the abutment. For the 15°, 30°, and 45° tests, the outward MSE wall movements became progressively asymmetric with greater displacement on the side opposite to the acute side of the abutment. For the 45° skew test, the outward MSE wall displacements on the side opposing the skew was 1.85 inches, while the displacement on the acute side was less than 0.25 inch. In this case the MSE reinforcements were too short to resist the pressures induced on the walls, and the entire soil mass in front of the skewed wall (including the reinforcements) was moving towards the MSE wall.

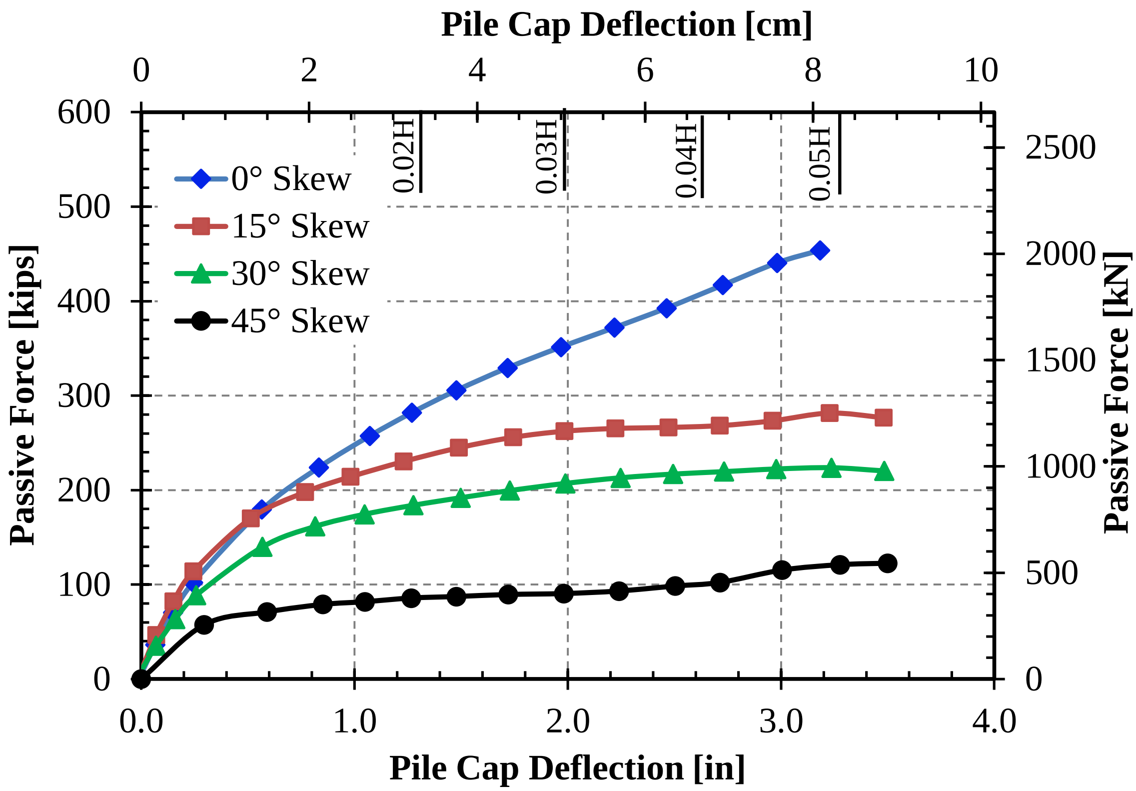

Fig. 12. Passive force-deflection curves for 0°, 15°, 30°, and 45° skew tests with 5.5-ft thick compacted sand backfill and MSE wingwalls parallel to direction of travel.

5.3 Tests with Parallel RC Tapered Wingwalls

Fig. 13 provides a plot of passive force-deflection curves for skew angles of 0° and 45° with the reinforced concrete tapered wingwalls parallel to the direction of travel (see wingwall geometry in Fig. 5). Both tests reached peak passive resistance at a deflection of about 0.045H, which is in the upper range of all previous full-scale tests. The peak passive force for the 45° skew curve is about 54% of that for the 0° skew, which is higher than would be expected (about 37%) based on previous 45° skew tests.

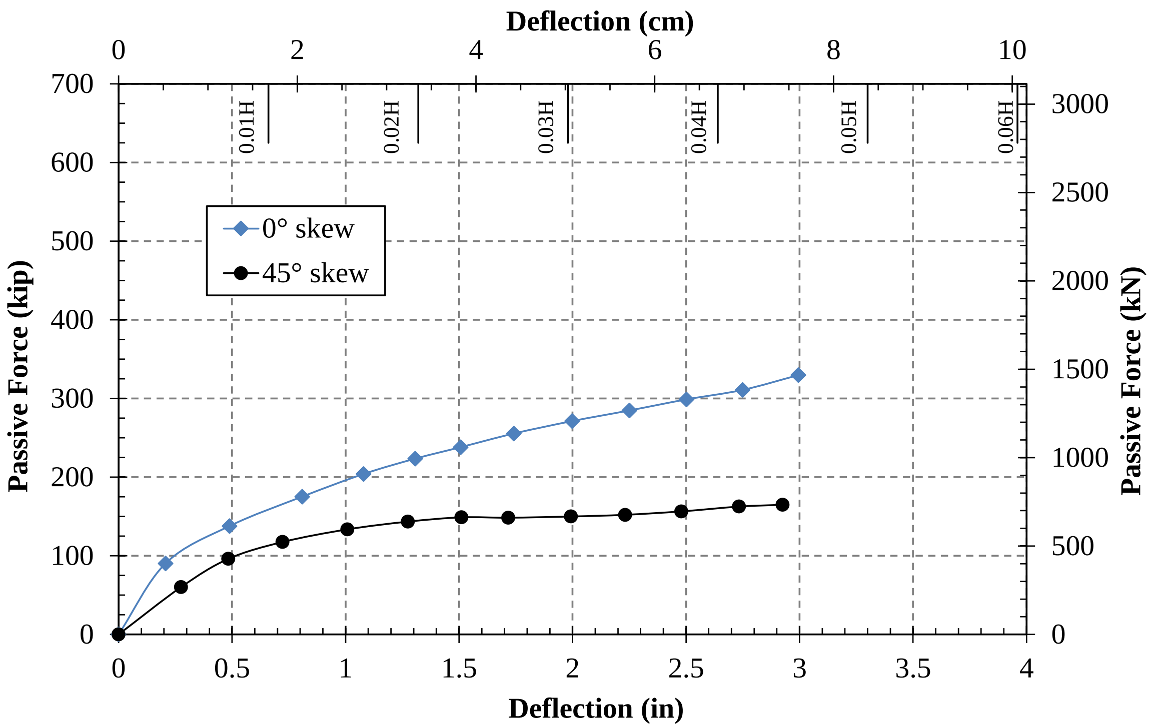

Fig. 13. Passive force-deflection curves for 0° and 45° skewed abutments with parallel tapered reinforced concrete (RC) wingwalls.

In this case, a wedge of soil between the wingwall and the abutment wall on the obtuse side became locked in place by wall friction on both walls and essentially moved uniformly with the abutment. This decreased the effective skew angle (to about 30°) leading to higher passive force than might be expected. Subsequent numerical analyses conducted by Snow (2019), using the 3D finite element computer code PLAXIS3D (Brinkgreve, 2015), replicated the observed behavior for the 11-ft wide abutment. However, additional analyses using PLAXIS3D, with a model of a 25-ft wide abutment, indicated that the influence of this wedge became small enough, relative to the overall width, that the increase in passive resistance was no longer significant. As a result, the computed reduction in passive force was consistent with expectations from previous testing (e.g. 35% of 0° skew passive force).

5.4 Tests with Transverse Wingwalls using Gravel and GRS Backfills

Passive force-deflection curves for skew angles of 0° and 30° from two tests with gravel backfill and two tests with Geosynthetic Reinforced Soil (GRS) with the same gravel backfill are all plotted together in Fig. 14. The passive force for the gravel backfills was considerably higher than that measured for sand backfills with similar geometries (Marsh et al. 2013, Rollins et al. 2015) owing to the higher friction angle (46º vs. 40º) and higher unit weight (145.1 lb/ft^3 vs. 117.8 lb/ft^3) of the gravel relative to the sand.

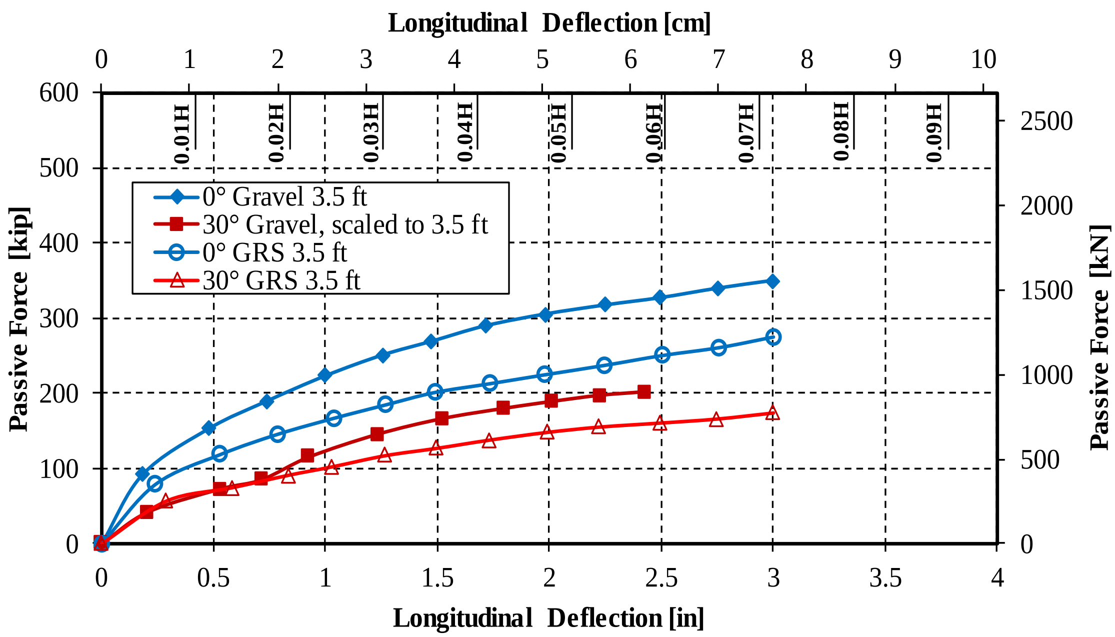

Fig. 14. Comparison of passive force-deflection curves for the gravel and Geosynthetic Reinforced Soil (GRS) backfill tests with skew angles of 0º and 30º.

Both pairs of tests involving gravel showed clear reduction in passive force due to skew angle—58% for the gravel tests and 63% for the GRS tests. The GRS gravel backfill was expected to yield higher passive resistance than unreinforced backfills because the shear failure plane would need to develop by passing through each geotextile layer. However, that was not the case for this set of tests as the geotextile had little effect on the shear resistance. The reduction in passive force for the GRS backfill compared to gravel was actually 21% at 7.6 cm (3.0 in) for the 0º tests and 13% for the 30º tests. The reduction in passive resistance was attributable to the reduced interface friction angle (wall friction) at the abutment wall produced by wrapping the geotextile around the gravel layers.

Perhaps most significantly, there was a decrease in stiffness in the GRS backfill, so that significantly higher deflections were required to reach equivalent passive resistances compared to the unreinforced gravel. This reduction in backfill stiffness can be favorable in the GRS Integrated Bridge System (IBS), or GRS-IBS, abutment configuration because it allows thermal movement without developing excessive induced stresses in the bridge superstructure.

The displacement required to develop the peak passive force was 0.06 to 0.07H for these gravel tests which was higher than the 0.03 to 0.05H range observed for tests in sand backfill. In a passive force-deflection test conducted on a pile cap with gravel backfill, Rollins and Sparks (2002) also reported a deflection of 0.06H to develop the passive resistance.

5.5 Skew Reduction Factor vs. Abutment Skew Angle

The peak passive force for each test in this study at a given skew angle was divided by the peak passive force for the zero skew case to determine the passive force reduction factor. These reduction factors from the full-scale field tests in this study are plotted versus skew angle in Fig. 15 along with reduction factors from large-scale lab tests (Rollins and Jessee 2013) and numerical analysis (Shamsabadi et al. 2006). The data points all fall within a fairly narrow band and are in very good agreement with the polynomial equation originally proposed by Rollins and Jessee (2013). Shamsabadi and Rollins (2014) proposed a simpler equation to define the passive force reduction factors as a function of skew angle:

$$R_{skew} = e^{-\theta/45^\circ} \tag{10}$$

where θ is the skew angle in degrees. Equation 10 is also plotted vs. skew angle in Fig. 15 in relation to the data points. This equation provides a very good fit with the data and has a correlation coefficient, R^2, of 0.96.

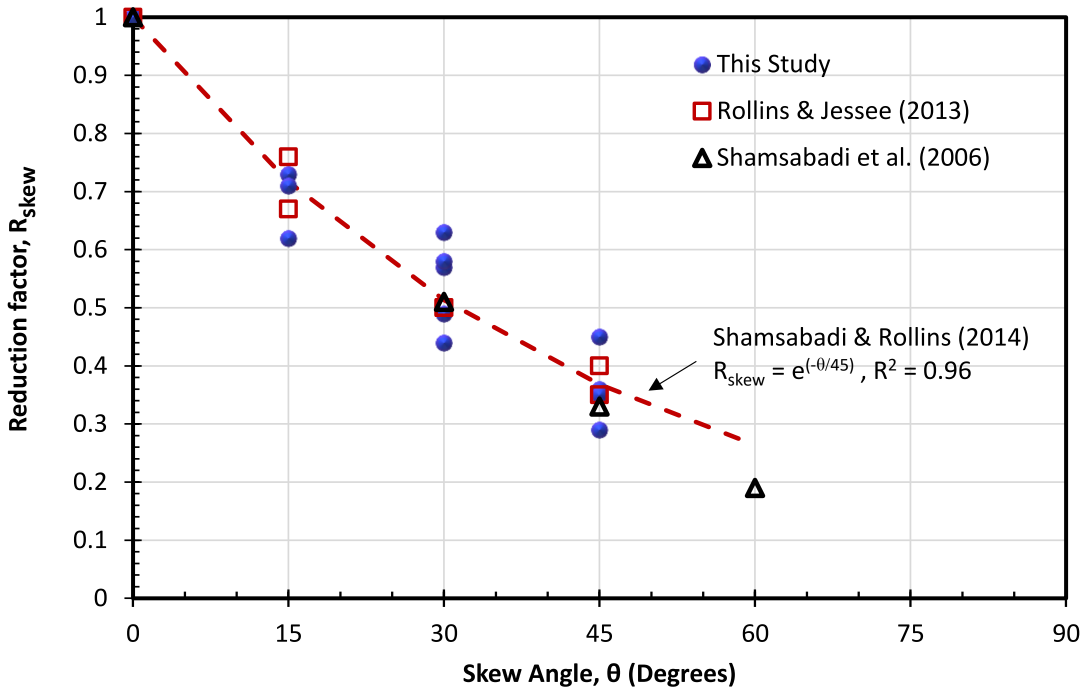

Fig. 15. Passive force reduction factor, R_{skew}, vs. skew angle for tests in this study, previous large-scale lab test (Rollins & Jessee 2013), and from numerical analyses (Shamsabadi et al. 2006) along with skew reduction factor equation (Shamsabadi and Rollins 2014).

6.0 NORMALIZED PASSIVE FORCE VERSUS DEFLECTION CURVES

In addition to defining the peak passive force as a function of the backfill height against the abutment, it is important to define the complete passive force-deflection curve for skewed bridge abutments. In the past, there was simply insufficient test data with which to define reliably the passive force-deflection curve; however, the many large-scale field tests conducted in this study make it possible to investigate the typical curve shape. Although design equations have generally defined the passive force-deflection curve using a linear or bi-linear approach (Caltrans 2001), the results from full-scale testing indicate that the curve is generally hyperbolic (see Figs. 7 through 13).

To develop a generic curve shape for cases where the backfill height against the abutment is variable, we have normalized the longitudinal deflection, Δ, by the backfill height, H, and we have normalized the passive force, P, by the peak passive force, P_{max}. Plots of the mean and one standard deviation normalized passive force vs. normalized deflection curves for all of the 14 tests in this study involving the sand backfill are plotted in Fig. 16.

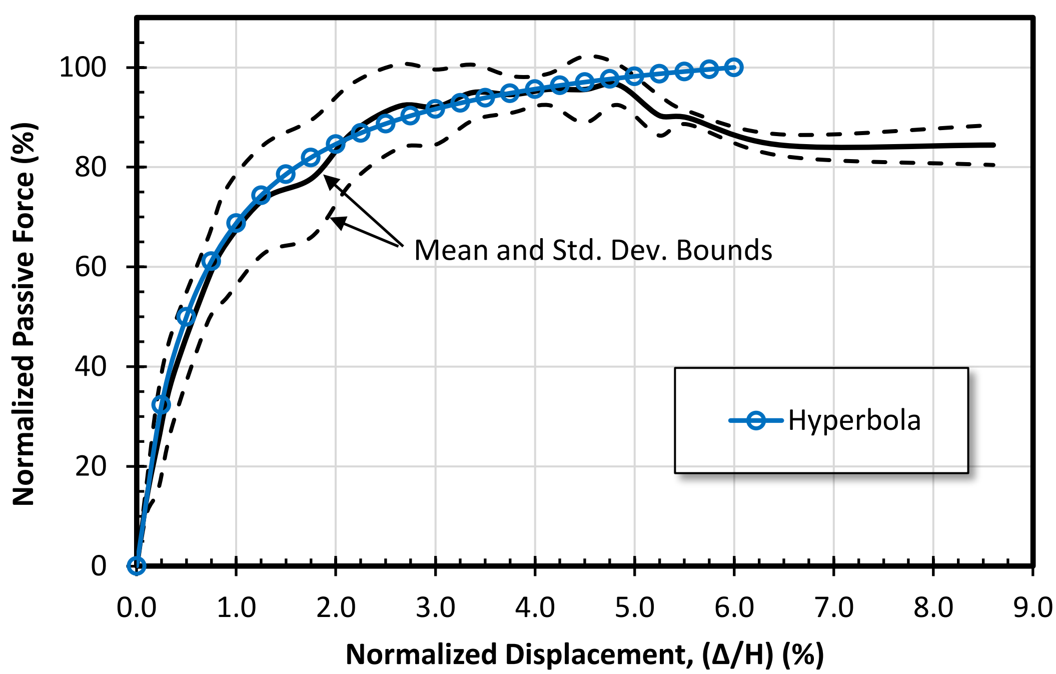

Fig. 16. Mean and one standard deviation normalized passive force vs. normalized longitudinal displacement curves based on 14 large-scale abutment lateral load tests conducted during this study along with best-fit hyperbola equation.

Despite the variation in skew angle, backfill height, and wingwall geometries (e.g. parallel, transverse, MSE), the resulting normalized curves form a relatively narrow band about the mean curve. The normalized passive force is between 92% and 98% between normalized displacements of 3% and 5%. This is consistent with the fact that peak passive force typically develops between a normalized displacement of 3% and 5%.

The normalized passive force tends to decrease somewhat at normalized displacements greater than about 5% with an average reduction of about 15%. However, it should be recognized that there are much fewer data points defining behavior beyond 5% displacement so these results should be viewed with some caution. As noted previously, soil compacted to more than about 97% of the modified Proctor maximum dry unit weight experienced some decrease in passive force as a result of soil dilation during shearing, but this was not the case for soils with relative compaction of 95%.

A generic curve shape has been developed to match the measured mean normalized passive force-normalized curve shape as shown in Fig. 16. The curve shape is a hyperbola given by the equation,

$$\frac{P}{P_{max}} = \frac{110\ (\Delta/H)}{[0.6 + \left(\frac{\Delta}{H}\right)]} \tag{11}$$

where (P/P_{max}) and (Δ/H) are both expressed as percentages. The agreement between the measured and computed curves is very good for almost all displacements up to 5% of H; however, the equation is unable to capture the post-peak reduction in normalized passive force. For the mean plus one standard deviation curve, replace the coefficient 110 with 115 and replace 0.6 with 0.5 from Eq. 11. For the mean minus one standard deviation curve, replace the coefficient 110 with 105 and replace 0.6 with 0.86 from Eq. 11.

7.0 SOIL-ABUTMENT INTERFACE FORCE INTERACTION

Fig. 17 provides a summary of the forces acting on the soil-abutment interface for the 0°, 15°, 30°, and 45° skew tests for the transverse wingwall tests with a 5.5-foot high sand backfill against the abutment wall. The longitudinal force is plotted against skew angle, along with passive force, applied shear force, and resisting shear force, as calculated by Eqs. 3, 4, and 5, respectively. In Eq. 5, ϕ was taken as 40° and cohesion was 100 psf. The passive force (P_P) decreases slightly more than the longitudinal force (P_L) with increased skew angle. Despite the decrease in applied longitudinal force, the applied shear force (P_T) still increases with skew angle while the shear resistance (P_R) decreases. At a skew angle of 30°, the shear resistance was approximately equal to the applied shear force. At an angle of 45° the shear resistance was less than the applied shear force, thus significant transverse sliding would have occurred without lateral resistance provided by the piles.

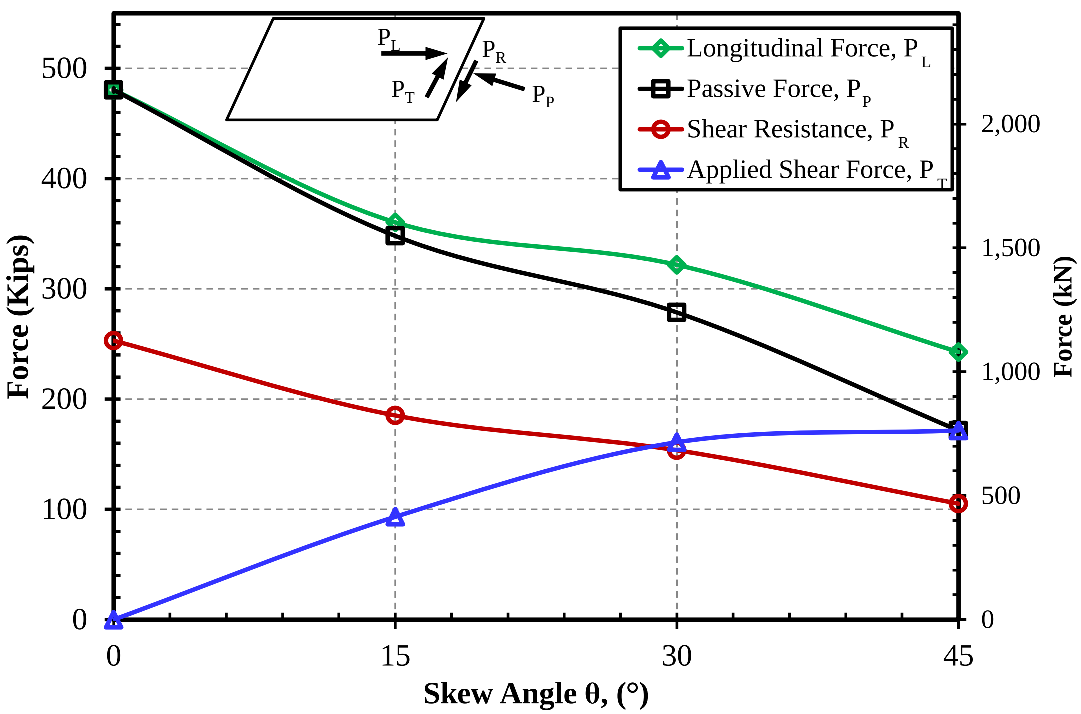

Fig. 17. Longitudinal, passive, applied shear, and resisting shear forces versus skew angle on the soil-abutment wall interface for 5.5-ft high sand backfill with transverse wingwalls.

As the applied shear force increased, relative to the shear resistance, movement of the pile cap in the transverse direction was required to mobilize shear resistance. Although deflections of both actuators were kept relatively consistent throughout the test to displace the pile cap longitudinally, transverse deflection still occurred as measured by the shape arrays. The transverse displacement progressively increased as the skew angle increased. The pile cap rotation was very small, less than 0.03°, for all tests and was unaffected by skew angle.

The relationship between the resisting shear force (P_R) and transverse cap displacement is plotted in Fig. 18. As skew angle increases, the maximum shear resistance decreases owing to the reduced passive force (see Eq. 5). However, in all cases the maximum shear resistance developed with transverse displacements of between 0.1 to 0.2 inch. This transverse displacement is consistent with the small movement (< 0.2 inch) necessary to develop side friction on pile shafts and vertical soil-abutment interfaces (Duncan and Mokwa, 2001).

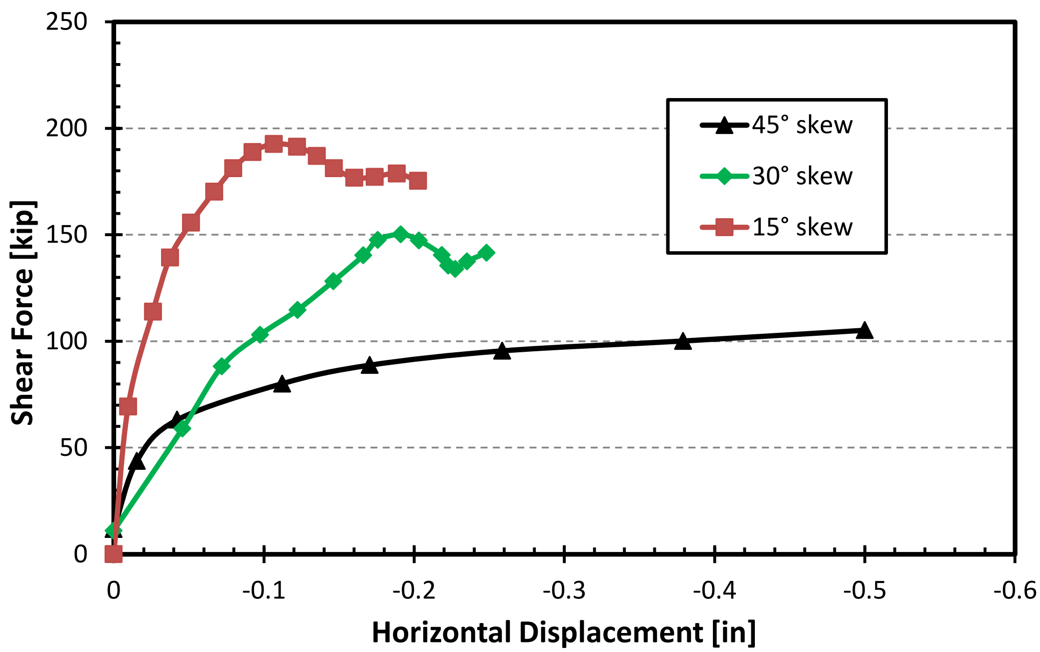

Fig. 18. Shear resistance vs. transverse displacement curves for skew angles of 15°, 30°, and 45° on the soil-abutment interface for 5.5-ft high sand backfill with transverse wingwalls.

8.0 SOIL-ABUTMENT EARTH PRESSURE DISTRIBUTION

Earth pressure distribution across the face of the pile cap was measured using six pressure plates as described previously. Although pressure cells are known to under-register or over-register the true earth pressure (Talesnick et al. 2020), they can also provide a qualitative indication of the pressure distribution. In this study we compared the passive force measured by the actuators with the passive force obtained from the measured pressure distribution to obtain an indication of accuracy. Fig. 19 shows the measured earth pressure distribution across the face of the skewed abutment for the 45° skew tests with transverse wingwalls, parallel MSE wingwalls, and parallel RC tapered wingwalls. The earth pressure distribution is shown for three or four different longitudinal pile cap displacement increments. Generally, the earth pressure is highest at the edges of the abutment wall and decreases towards the center. Because the pile cap is displacing uniformly in the longitudinal direction, the increase is not attributable to pile rotation. The higher earth pressures at the edge are likely similar to the higher bearing pressures at the edge of a rigid footing predicted by elastic theory (Hegger et al. 2007).

Fig. 20 shows the measured earth pressure distribution at five pressure cells across the face of the skewed abutment for the 30° skew tests with a 5.5-ft backfill for the transverse wingwalls and parallel MSE wingwalls along with the 3.0-ft backfill with transverse wingwalls. The earth pressures start out fairly uniform across the abutment for smaller longitudinal abutment deflections. However, at larger abutment deflections, the pressures increase at the edges of the abutment and become lower near the center as expected based on elastic theory. The earth pressures were not consistently higher on one edge or the other, which is expected because the abutment was being pushed longitudinally into the backfill with minimal rotation. Small variations in pile cap rotation were likely responsible for the variations in peak pressure.

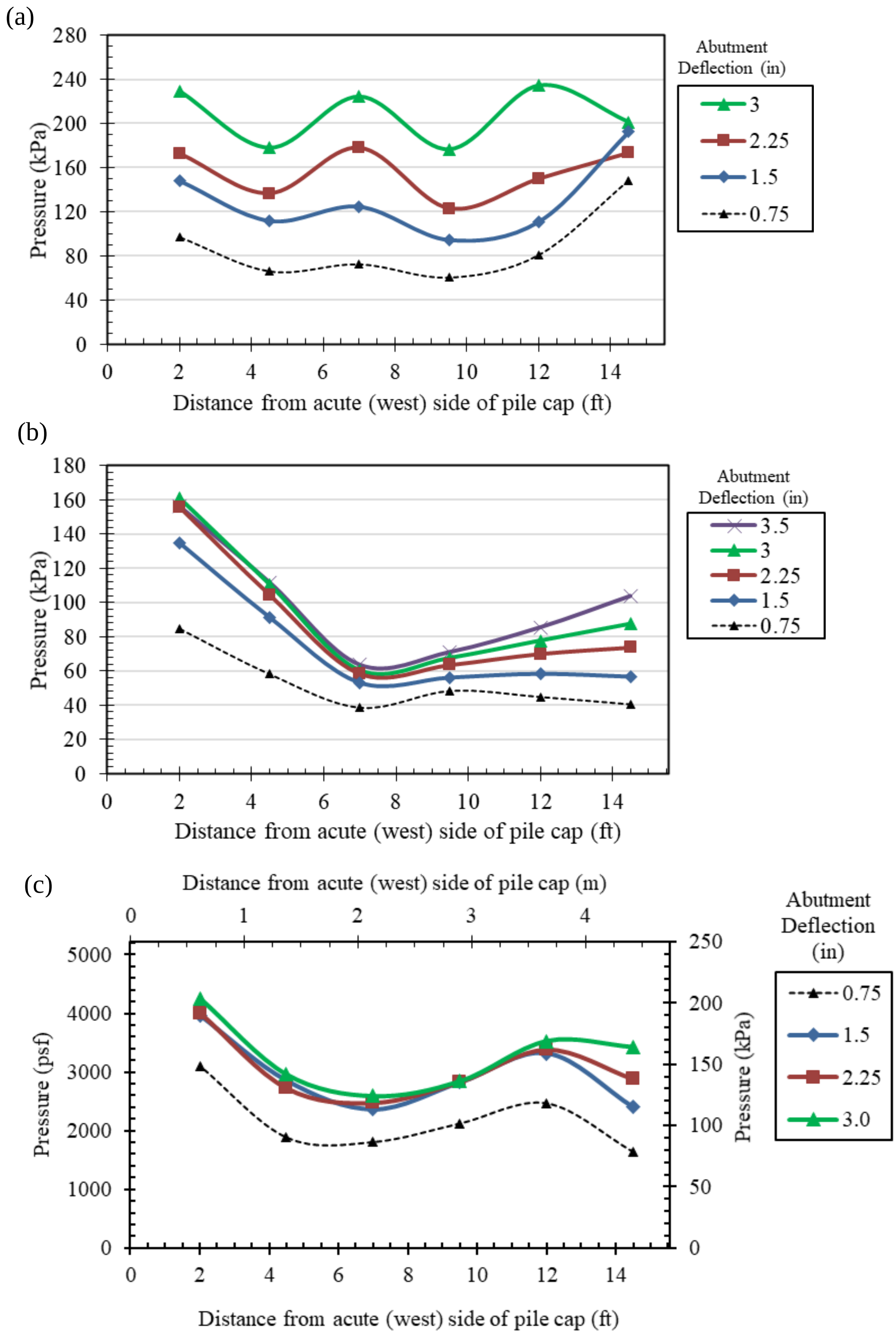

Fig. 19. Measured earth pressure on abutment wall for 45° skew tests and 5.5-ft backfill with (a) transverse wingwalls, (b) parallel MSE wingwalls, and (c) parallel tapered RC wingwalls.

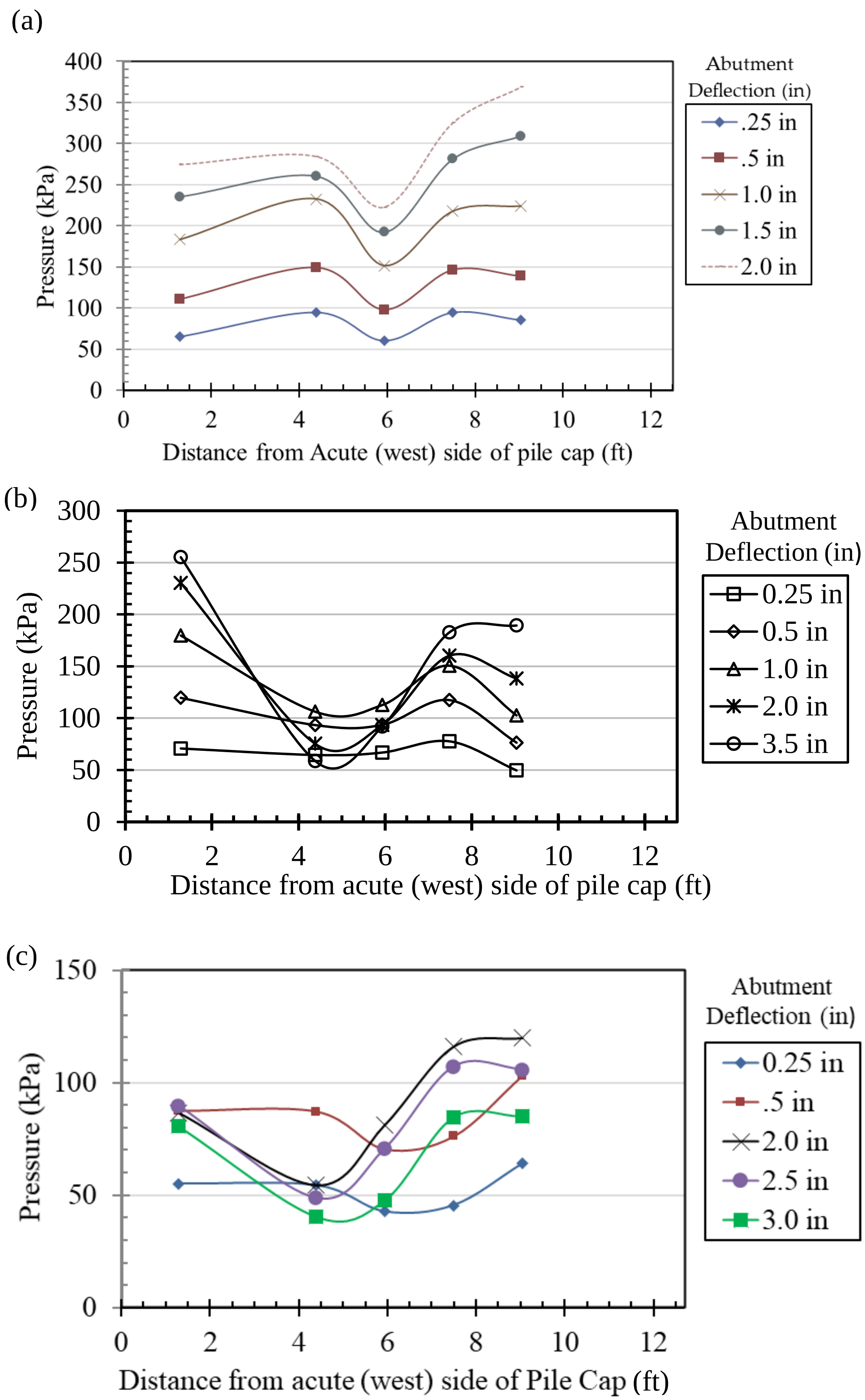

Fig. 20. Measured earth pressure on abutment wall for 30° skew tests and 5.5-ft backfill with (a) transverse wingwalls and (b) parallel MSE wingwalls along with (c) 3.0-ft backfill with transverse wingwalls.

Fig. 21 provides measured earth pressure distribution at six pressure cells across the face of the skewed abutment for a 30° skew test with a 5.5-ft sand backfill and parallel concrete wingwalls. These wingwalls simulate the 2D geometry that would be typical of a wide bridge abutment (e.g. 75 to 125 feet wide). In this test, the actuator on the east (right) side of the abutment was forced to deflect 0.25 to 0.5 inch more than the actuator on the west side. This created a rotation angle of 0.11° to 0.30° which is typical of the rotation of skewed bridge superstructures (0.12° to 0.5° or 0.002 to 0.009 radians) based on investigations by Prof. Ian Buckle at University of Nevada, Reno (Personal communication 2016).

At small abutment deflections (0.65 inch), the earth pressure was relatively uniform. However, at larger deflections, the earth pressure became higher on the east (right) side, which is the side that displaced into the backfill first. This is also the side of the abutment which would be expected to rotate into the backfill for a typical skewed abutment.

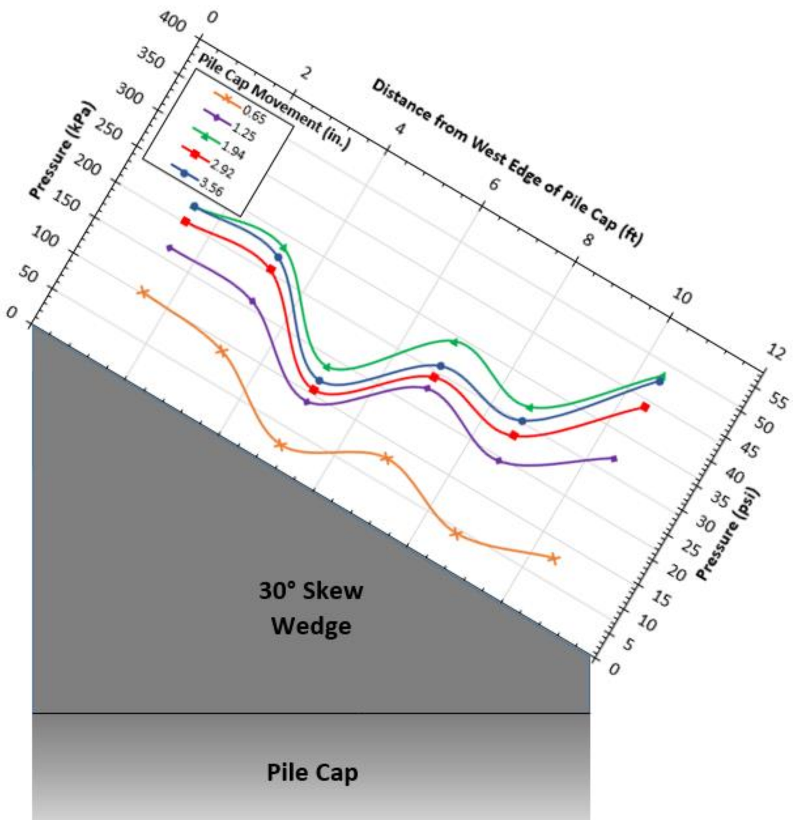

Fig. 21. Measured earth pressure on abutment wall for 30° skew test with 5.5-ft sand backfill and parallel concrete wingwalls loaded at an angle of about 0.2 degrees relative to the direction of travel. This rotation is typical of that for skewed bridge superstructures.

9.0 PASSIVE FAILURE SURFACE GEOMETRY AND BEHAVIOR

Post-failure trenching identified the location of the passive shear surface in vertical red sand columns for the tests in sand. A typical measured failure surface is plotted versus distance behind the abutment wall in Fig. 22(a) along with failure surfaces predicted by the log-spiral, Coulomb, and Rankine failure theories. Clearly, the log-spiral theory provides the best agreement with the measured failure surface while Rankine and Coulomb surfaces grossly under- and over-estimate the volume and shape of the passive wedge, respectively. In addition to the basal shear surface, a shear plane was detected extending diagonally from the top of the abutment wall to the basal failure surface. This diagonal shear plane appears to be the boundary between the Prandtl and Rankine failure zones as identified in the schematic drawing of the log-spiral geometry in Fig. 22(b). In plan view for the transverse wingwalls in the zero skew tests, the failure surface daylighted symmetrically about the center of the abutment; however, for the skew tests, the failure surface was asymmetric and extended further beyond the edge of the acute side.

For the densely compacted soils in this study, the backfill soil behind the wall heaved upward within the passive failure zone as shown in Fig. 22(a) as the abutment was pushed into the backfill. Peak heave was typically between 2 and 3% of the backfill height. String potentiometers in the backfill indicated that the passive failure zone largely moved as a block with little compressive strain; however, compressive strains of 2 to 5% occurred in a two-foot zone immediately behind the abutment wall and in the two-foot zone where the failure surface daylighted, compressing against the backfill behind the shear surface.

(a)

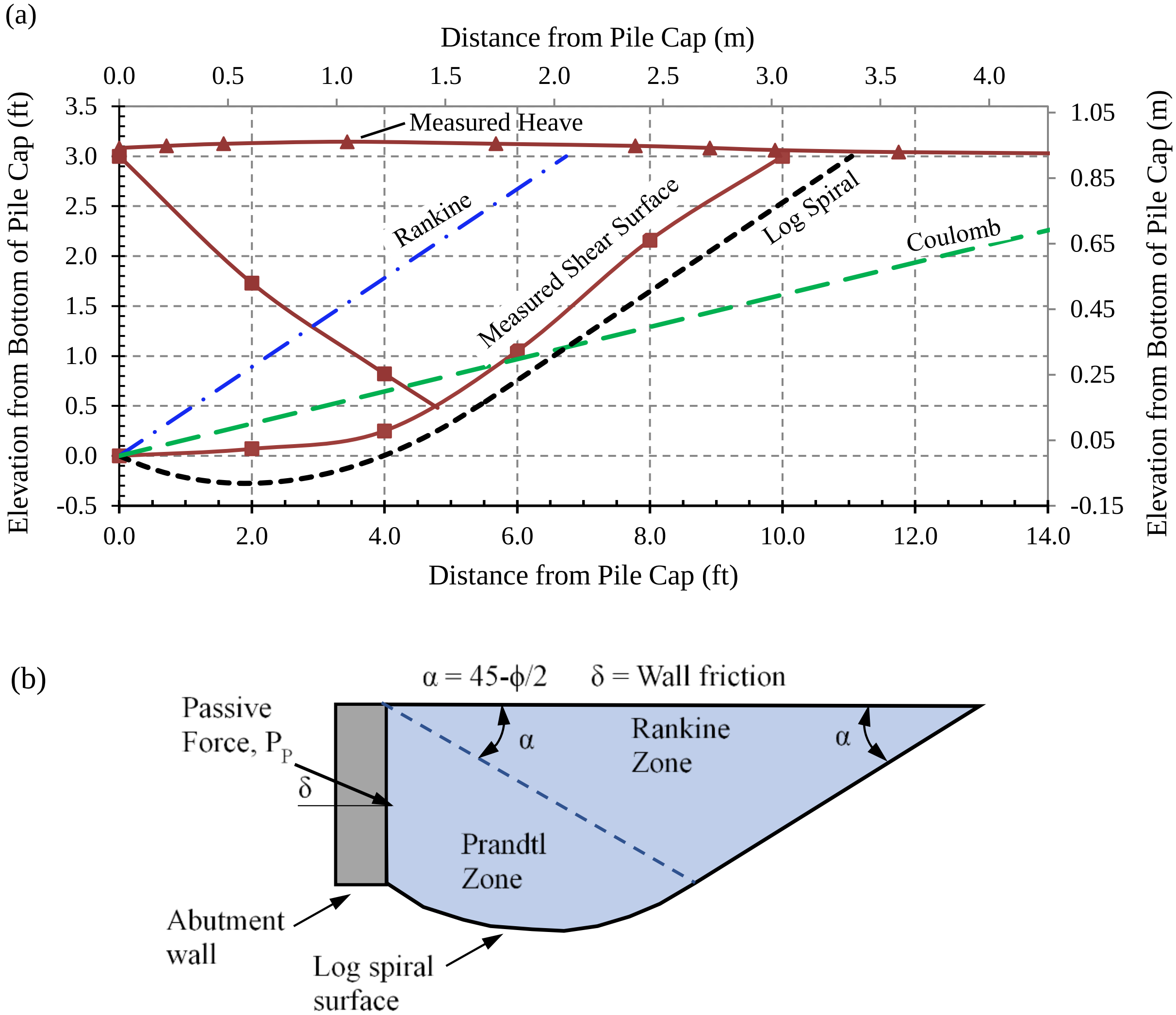

Fig. 22. Comparison of (a) measured and computed passive failure surfaces and (b) diagram of log-spiral failure surface geometry.

10.0 CONCLUSIONS

This report summarizes the results of the testing and analyses performed for the large-scale tests of Phase I of the TPF-5(264) pooled fund study. Detailed reports on each of the large-scale tests are available from the Utah Department of Transportation Research & Innovation Division and the TPF-5(264) study webpage. We anticipate that the main conclusions from the testing and analyses, listed below, will be useful for implementation, improved design methods, and further research by structural and geotechnical engineers.

1. For abutments with transverse wingwalls, the passive failure surface extends beyond the width of the abutment. The effective width of the shear plane can be reasonably estimated using the Brinch-Hansen equation to compute a 3D correction factor. This factor becomes less important as the abutment width increases.
2. For abutments with parallel wingwalls provided by MSE walls, the passive failure plane becomes essentially a 2D or plane strain failure. In this case, the plane strain friction angle, which is typically 12% higher than the triaxial friction angle, is necessary to obtain agreement with the measured passive force.
3. The passive force for bridge abutments is best predicted using the log-spiral method with proper accounting of interface friction, plane strain conditions, and effective width of the passive shear wedge.
4. Results from this large-scale field study confirm that passive force decreases significantly as the abutment skew angle increases as observed previously in small-scale lab test results (Rollins and Jessee 2013) and numerical studies (Shamsabadi et al. 2006).
5. The passive force reduction equation originally proposed by Rollins and Jessee (2013) and a simpler equation proposed by Shamsabadi and Rollins (2014) provide reasonable estimates of the measured passive force reduction in densely compacted granular material. This reduction factor was was not affected by the backfill material (gravel or sand), the backfill width-to-height ratio, or the wingwall type.
6. Normalized passive force vs. normalized deflection curves for all of the tests in sand with variable skew angles plot within a narrow band with peak resistance developing at

longitudinal abutment deflections between 3% to 5% of the backfill heights. The mean and one standard deviation bound curves were best modeled by using a hyperbola.

7. The longitudinal abutment displacement required to develop the peak passive force for sand compacted to 95% of the modified Proctor maximum dry unit weight was between 3% and 5% of backfill height, consistent with previous large-scale tests (Duncan and Mokwa 2001, Rollins and Cole 2006, Lemnitzer et al. 2009). However for gravel backfills, displacement equal to 6% to 7% of the backfill height was necessary to mobilize full passive resistance similar to that observed in gravel by Rollins and Sparks (2002).
8. The transverse displacement required to develop the full shear resistance on the abutment wall was typically between 0.1 to 0.2 inch which is consistent with displacements necessary to mobilize side friction on piles.
9. The passive pressure distribution on the abutment wall was typically higher on the edges than in the center when the pile cap was loaded longitudinally into the backfill, consistent with the higher bearing pressure on rigid footings predicted by elastic theory (Hegger et al. 2007). When the pile cap was allowed to rotate during loading, the pressures were highest on the obtuse side of the abutment.
10. The passive failure plane in the backfill soil typically had a shape similar to that predicted by the log-spiral method with a Prandtl log-spiral section and a Rankine failure wedge. This failure wedge tends to move as a block; however, significant compressive strains (3 to 4%) occurred in the backfill soil two feet directly behind the abutment and near the location where the failure surface daylights. Ground heave was typically 2 to 3% of the backfill height and occurred within the passive failure zone.

REFERENCES

Burke, M. P., Jr. "Semi-integral bridges: movements and forces." *Transportation Research Record: Journal of the Transportation Research Board*, 1994; 1460, 1-7.

Brinch Hansen, J. “Resistance of a rectangular anchor slab.” Bull. No. 21, *Danish Geotechnical Institute*, Copenhagen, Denmark, 1966. 12-13.

Brinkgreve, R.B.J. “Reference Manual: PLAXIS 3D-2015.” Delft University of Technology & PLAXIS b.v.; The Netherlands

Cole, R., and Rollins, K. "Passive earth pressure mobilization during cyclic loading." *Journal of Geotechnical and Geoenvironmental Engineering*, 2006; 132(9): 1154-1164.

Duncan, J., and Mokwa, R. "Passive earth pressures: theories and tests." *Journal of Geotechnical and Geoenvironmental Engineering*, 2001, 127(3): 248-257.

Franke, B.W., Rollins, K.M., Marsh, A.K., Smith, J., Palmer, K. “Passive force-deflection behavior for skewed abutments with mse wingwalls", Procs. *7th National Seismic Conf. on Bridges and Highways*, FHWA, 2013. 12 p.

Hegger, J., Ricker, M., Ulke, B., & Ziegler, M. “Investigations on the punching behaviour of reinforced concrete footings.” *Engineering Structures*, 2007. 29(9), 2233 – 2241.

Heiner, L., Rollins, K.M. and Gerber, T.G. “Passive force-deflection curves for abutments with MSE confined approach fills.” Procs. 6th National Seismic Conference on Bridges, Charleston, South Carolina, Federal Highway Administration, CD-Rom, 2008. 12 p.

Kulhawy, F. H., and Mayne, P. W. “Manual on estimating soil properties for foundation design.” *Electric Power Research Institute*, EPRI EL-6800, Project 1493-6 Final Report, 1990, 298 p.

Lee, K. L., and Singh, A. "Relative density and relative compaction." *Journal of Soil Mechanics and Foundations Design,* 1971**,** 97(7): 1049-1052.

Lemnitzer, A., Ahlberg, E., Nigbor, R., Shamsabadi, A., Wallace, J., and Stewart, J. "Lateral performance of full-scale bridge abutment wall with granular backfill." *Journal of Geotechnical and Geoenvironmental Engineering*, ASCE, 2009, 135(4): 506-514.

Marsh, A.K., Rollins, K.M., Franke, B., Smith, K., and Palmer, K. "Passive force-deflection behavior for zero and thirty degree skewed abutments", *Transportation Research Record*, FHWA, 2013.

Rollins, K.M. and Cole, R.T. “Cyclic Lateral Load Behavior of a Pile Cap and Backfill.” *J. Geotechnical and Geoenvironmental Engrg*., ASCE, 2006, 132(9), 1143-1153.

Rollins, K. M., Palmer, K. and Fredrickson “Performance of skewed abutments from large-scale testing” *Procs. IFCEE 2015,* ASCE, 2015. 267-1277.

Rollins, K. M., and Jessee, S. J. "Passive force-deflection curves for skewed abutments." *Journal of Bridge Engineering*; 18 (10): 2013, 1086-1094

Rollins, K., and Sparks, A. "Lateral resistance of full-scale pile cap with gravel backfill." *Journal of Geotechnical and Geoenvironmental Engineering*, 2002; 128(9), 711-723.

Shamsabadi, A. and Rollins, K.M. “Three-dimensional nonlinear continuum seismic soil-structure interaction analysis of skewed bridge abutments.” *Procs., Eighth European Conference on Numerical Methods in Geotechnical Engineering*, 2014. Delft, the Netherlands, 6 p.

Shamsabadi, A., Kapuskar, M., a Skend Zand, A. "Three-dimensional nonlinear finite-element soil-abutment structure interaction model for skewed bridges." *Fifth National Seismic Conference on Bridges & Highways*, 2006; San Francisco, CA, 14.

Shamsabadi, A., Dasmeh, A., Nojoumi, A., Rollins, K.M and Taciroglu, E. “Lateral capacity model for backfills reacting against skew-angled abutments under seismic loading” J. Geotechnical & Geoenvironmental Engrg., ASCE, 2019. 146(2), https://doi.org/10.1061/(ASCE)GT.1943-5606.0002183

Snow, S.K. “Numerical analysis of passive force on skewed bridge abutments with reinforced concrete wingwalls.” MS. Thesis, *Civil & Environmental Engineering Dept., Brigham Young University*, Provo, UT, 2009. 113 p.

Talesnick, M., Ringel, M., and Rollins, K. (2020). “Development of a hybrid soil pressure sensor and its application to soil compaction.” Canadian Geotechnical Journal https://doi.org/10.1139/cgj-2020-0272

Toro, F., Rubilar, F., Hube, M.A., Santa-Maria, H., and Cabrera, T. "Statistical analysis of underpasses during 2010 Chile earthquake". Procs. *7th National Seismic Conf. on Bridges and Highways*, FHWA, 2013. 12 p.